

GEOMECHANICAL WELLBORE STABILITY ASSESMENT FOR
SAYINDERE, KARABOĞAZ, KARABABA FORMATIONS IN X FIELD

A THESIS SUBMITTED TO
THE GRADUATE SCHOOL OF NATURAL AND APPLIED SCIENCES
OF
MIDDLE EAST TECHNICAL UNIVERSITY
BY
TEVHİDE TUĞBA UYAR

IN PARTIAL FULFILLMENT OF THE REQUIREMENTS
FOR
THE DEGREE OF MASTER OF SCIENCE
IN
PETROLEUM AND NATURAL GAS ENGINEERING

JUNE 2011

Approval of the thesis:

**GEOMECHANICAL WELLBORE STABILITY ASSESMENT FOR
SAYINDERE, KARABOĞAZ, KARABABA FORMATIONS IN X FIELD**

submitted by **TEVHİDE TUĞBA UYAR** in partial fulfillment of the requirements
for the degree of **Master of Science in Petroleum and Natural Gas Engineering
Department, Middle East Technical University** by,

Prof. Dr. Canan Özgen
Dean, Graduate School of **Natural and Applied Sciences** _____

Prof. Dr. Mahmut Parlaktuna
Head of Department, **Petroleum and Natural Gas Engineering** _____

Prof. Dr. Mustafa Verşan Kök
Supervisor, **Petroleum and Natural Gas Engineering Dept., METU** _____

Examining Committee Members:

Prof. Dr. Mahmut Parlaktuna
Petroleum and Natural Gas Engineering Dept., METU _____

Prof. Dr. Mustafa Verşan Kök
Petroleum and Natural Gas Engineering Dept., METU _____

Prof. Dr. Nurkan Karahanoğlu
Geological Engineering Dept., METU _____

Dr. Reha Özel
TPAO Research Center _____

Selçuk Erkeköl, M.Sc.
TPAO Research Center _____

Date: 24.06.2011

I hereby declare that all information in this document has been obtained and presented in accordance with academic rules and ethical conduct. I also declare that, as required by these rules and conduct, I have fully cited and referenced all material and results that are not original to this work.

Name, Last Name: TEVHİDE TUĞBA UYAR

Signature:

ABSTRACT

GEOMECHANICAL WELLBORE STABILITY ASSESMENT FOR SAYINDERE, KARABOĞAZ, KARABABA FORMATIONS IN X FIELD

Uyar, Tevhide Tuğba

M.Sc., Department of Petroleum and Natural Gas EGINEERING

Supervisor: Prof.Dr. Mustafa Verşan K k

June 2011, 82 pages

Wellbore stability problems make up huge over-costs worldwide. Since in recent years declining resource volumes and favorable oil prices are encouraging operators to drill deeper, more complex well trajectories drilling for hydrocarbons have turn into a much more challenging task. Furthermore, the complexity and variations of those wells have added the weight to planning and problem anticipation at both drilling and production stages.

The thesis will describe the geomechanical wellbore stability analysis of Sayındere, Karaboğaz and Karababa formations drilled in X field, Adıyaman. The analysis assumes validity of linear elastic theory for porous media and requires drilling reports, well logs, laboratory tests and core analysis.

It was observed that with the assessment of geomechanical wellbore stability analysis mud weight window, which includes minimum mud weight and maximum mud weight can be determined for the studied formations.

Keywords: Wellbore stability, acoustic logs, dynamic elastic rock strength parameters, mud weights

ÖZ

X SAHASI SAYINDERE, KARABOĞAZ ve KARABABA FORMASYONLARI İÇİN JEOMEKANİK KUYU STABİLİTESİ DEĞERLENDİRMESİ

Uyar, Tevhide Tuğba

Yüksek Lisans, Petrol ve Doğalgaz Mühendisliği Bölümü

Tez Yöneticisi: Prof.Dr. Mustafa Verşan Kök

Haziran 2011, 82 sayfa

Kuyu stabilitesi ile ilgili problemler bütün dünyada yüksek maddi zararlara neden olmaktadır. Azalan kaynaklar ve yüksek petrol fiyatları yatırımcıları daha derin ve kompleks rezervuarlara, daha zorlu kuyu şekillerine yönlendirmekte, hidrokarbon hedefli sondajlar daha zorlu bir iş haline gelmektedir. Bu kuyuların karmaşıklığı ve çeşitliliği, sondaj planlama ve problem çözme aşamalarının önemini artırmaktadır.

Bu çalışma Adıyaman-X sahasında Sayındere, Karaboğaz ve Karababa formasyonları için jeomekanik kuyu stabilitesi analizi yapılmıştır. Uygulanan yöntemde gözenekli ortamda lineer elastik teorisinin geçerli olduğu varsayılmakta, günlük sondaj raporları, kuyu logları, laboratuvar ve karot analizleri kullanılmaktadır.

Çalışmanın sonucunda jeomekanik kuyu stabilitesi analiz yöntemi değerlendirilmiş, ele alınan formasyonlar için minimum-maksimum çamur ağırlığı aralığı verilmiştir.

Anahtar Kelimeler: Kuyu stabilitesi, akustik loglar, dinamik elastik kayaç mukavemet parametreleri, çamur ağırlığı

To My Family,

ACKNOWLEDGEMENTS

I would like to express my sincere thanks to my supervisor Prof. Dr. Mustafa Verşan K k for his academical help and guidance. I would like to thank Filiz Şahin, Reha  zel, Yıldız Karakeçe for their suggestions and comments. It is a pleasure to thank my colleague Gazel Tekdal to support me. I also want to thank TPAO Research Center Rock Mechanics and Geochemistry Laboratories for the experiments. I express my gratitude to Turkish Petroleum Corporation for permission to reproduce well logs, experiment results and well data.

Lastly, I am heartily thankful to my husband Arda Uyar for his help and understanding.

TABLE OF CONTENTS

| | |
|---|------|
| ABSTRACT | iv |
| ÖZ | v |
| ACKNOWLEDGEMENTS | vii |
| TABLE OF CONTENTS..... | viii |
| LIST OF TABLES | xii |
| LIST OF FIGURES | xiii |
| LIST OF SYMBOLS | xv |
| CHAPTERS | |
| 1. INTRODUCTION | 1 |
| 2. THEORY | 3 |
| 2.1 In Situ Stresses | 3 |
| 2.1.1 Stress in the Subsurface | 3 |
| 2.1.1.1 Vertical Principal Stress | 6 |
| 2.1.1.2 Horizontal Principal Stresses | 6 |
| 2.1.2 Downhole Stressors..... | 8 |
| 2.1.2.1 Pore Pressure..... | 9 |
| 2.1.2.2 Temperature Differences | 9 |
| 2.1.2.3 Chemical Interactions..... | 10 |
| 2.1.3 Changes in Stress | 10 |
| 2.2 Well Logging | 14 |
| 2.2.1 Gamma Ray (Gr) Log | 14 |
| 2.2.2 Density Log..... | 17 |
| 2.2.3 Neutron Log | 17 |

| | |
|---|----|
| 2.2.4 Sonic Log | 17 |
| 2.2.5 Borehole Acoustic Waves | 18 |
| 2.2.5.1 P-Waves | 19 |
| 2.2.5.2 S-Waves | 20 |
| 2.2.5.3 Ray Tracing..... | 20 |
| 2.2.5.4 Stoneley Waves | 21 |
| 2.3 Laboratory Tests..... | 23 |
| 2.3.1 Core Representativeness, Size Effects, Core Alteration | 23 |
| 2.4 Linear Elastic Theory | 24 |
| 2.4.1 The Mohr-Coulomb Criterion | 24 |
| 2.4.2 Uniaxial Compressive Strength..... | 27 |
| 3. EXPERIMENTAL SECTION | 29 |
| 3.1 Lithology Identification | 29 |
| 3.1.1 Drill Cuttings..... | 29 |
| 3.1.2 M-N Plot | 30 |
| 3.1.3 XRD Analysis | 33 |
| 3.2 Dynamic Elastic Properties | 34 |
| 3.3 Laboratory Tests..... | 36 |
| 3.3.1 Specific Gravity Measurement..... | 36 |
| 3.3.2 Density determination of solid matter by Pycnometer..... | 37 |
| 3.3.3 Shear and Compressional Time Measurement by Sonic Viewer..... | 39 |
| 3.3.3.1 Ultrasonic Velocity Measuring System for Rock Sample | 39 |
| 3.3.4 Uniaxial Compressive Strength Measurement..... | 40 |
| 3.4 Borehole Failure Criteria..... | 41 |
| 3.4.1 Vertical, Impermeable Borehole in a Linear Elastic Formation (with no porosity) | 41 |

| | |
|--|----|
| 3.4.1.1 Shear failure | 42 |
| 3.4.1.2 Tensile failure..... | 44 |
| 3.4.2 Vertical, Impermeable Borehole in a Linear Elastic Formation (with porosity) | 44 |
| 3.4.2.1 Shear Failure | 44 |
| 3.4.2.2 Tensile failure..... | 45 |
| 3.4.3 Permeable Borehole | 46 |
| 3.4.4 Effect of Non-linearity | 47 |
| 3.4.5 Evaluation of Input Data | 47 |
| 4. STATEMENT OF PROBLEM | 49 |
| 5. RESULTS AND DISCUSSION | 50 |
| 5.1 Well Information | 50 |
| 5.2 Formation Information and Lithology Identification..... | 53 |
| 5.2.1 Formation Information | 53 |
| 5.2.1.1 Sayındere Formation | 53 |
| 5.2.1.2 Karaboğaz Formation..... | 53 |
| 5.2.1.3 Karababa Formation..... | 53 |
| 5.2.2 Lithology Information..... | 54 |
| 5.3 Elastic Constants of Sayındere, Karaboğaz and Karababa Formations | 58 |
| 5.3.1 Elastic Constants by Well Logs | 58 |
| 5.3.2 Sample Calculation of Dynamic Elastic Parameters..... | 61 |
| 5.3.2 Elastic Constants by Laboratory Tests..... | 63 |
| 5.4 Calculation of Minimum and Maximum Mud Weights..... | 65 |
| 5.4.1 Sample calculation | 70 |
| 5.4.1.1 Calculation of Minimum Required Mud Weight..... | 71 |
| 5.4.1.2 Calculation of Maximum Allowable Mud Weight | 74 |

| | |
|---------------------|----|
| 6. CONCLUSIONS..... | 77 |
| REFERENCES..... | 79 |

LIST OF TABLES

TABLES

| | |
|---|----|
| Table 1 Values of M and N for common minerals..... | 31 |
| Table 2 Elastic rock parameters | 35 |
| Table 3 XRD analysis result | 58 |
| Table 4 Generalized bulk density and ts/tc values | 63 |
| Table 5 Measured values of density and ts/tc | 64 |
| Table 6 Elastic parameters for X-11 well | 65 |
| Table 7 Uniaxial compressive strength and cohesion angles | 69 |
| Table 8 Maximum mud weights from laboratory tets..... | 69 |

LIST OF FIGURES

FIGURES

| | |
|---|----|
| Figure 1 In situ stresses; σ_H for larger horizontal stress, σ_v for vertical stress and σ_h for smaller horizontal stress. | 4 |
| Figure 2 Stress-strain diagram | 5 |
| Figure 3 Schematic hydraulic fracturing test | 7 |
| Figure 4 Chart of a leak-off test | 8 |
| Figure 5 Stresses before and after drilling | 11 |
| Figure 6 Tensile failure | 12 |
| Figure 7 Shear failure..... | 13 |
| Figure 8 Total wave train and components | 18 |
| Figure 9 P-waves, S-waves, Stoneley waves. | 22 |
| Figure 10 Mohr-Coulomb criterion in τ - σ space. | 25 |
| Figure 11 Stress versus deformation in a uniaxial compression test | 27 |
| Figure 12 M-N plot for several minerals | 32 |
| Figure 13 X Ray Diffractometer | 33 |
| Figure 14 Pycnometer | 38 |
| Figure 15 Experimental set-up..... | 38 |
| Figure 16 Sonic viewer | 39 |
| Figure 17 Field location in map | 51 |
| Figure 18 Well locations | 51 |
| Figure 19 X-12 Well stratigraphic column | 52 |
| Figure 20 Drill cuttings report | 54 |
| Figure 21 Available Well Logs for X-12 Well | 55 |
| Figure 22 M-N plot for Sayindere formation..... | 56 |
| Figure 23 M-N plot for Karaboğaz formation..... | 57 |
| Figure 24 M-N plot for Karababa formation..... | 57 |
| Figure 25 A section from the DSI log | 59 |
| Figure 26 Shear and compressional velocities | 60 |

| | |
|--|----|
| Figure 27 Shear modulus for Sayındere, Karaboğaz and Karababa formations | 60 |
| Figure 28 X-11 Well cores and sample places..... | 64 |
| Figure 29 X-12 Min-Max mud weights | 67 |
| Figure 30 X-12 Formation integrity test graph | 68 |

LIST OF SYMBOLS

| | |
|--------------------------------|--|
| Φ | friction angle |
| ϕ | porosity |
| ϕ_N | neutron porosity |
| ε | strain |
| ν | Poisson's ratio |
| α | Biot constant |
| β | failure angle |
| τ | shear stress |
| ρ_b | actual bulk density |
| ρ_f | density of pore fluid |
| ρ_i | density of each radioactive mineral |
| σ | stress, normal stress |
| σ' | effective stress |
| σ_θ | tangential stress |
| $\sigma_1, \sigma_2, \sigma_3$ | principal stress |
| σ_h | horizontal stress, minor horizontal stress |
| σ_H | major horizontal stress |

| | |
|-----------------------------------|--|
| σ_r | radial stress (confining stress in triaxial tests) |
| σ_v | vertical stress |
| $\sigma_x, \sigma_y, \sigma_z$ | components of normal stress |
| $\tau_{xy}, \tau_{xz}, \tau_{yz}$ | components of shear stress |
| A | atomic weight |
| A | area |
| A_i | proportionality factor of each |
| c_b | bulk compressibility |
| c_r | rock compressibility |
| CNL ϕ | CNL log porosity |
| CNL ϕ_{sh} | CNL porosity for maximum shale point |
| c_o | uniaxial compressive strength |
| E | Young's modulus |
| F | force |
| G | shear modulus |
| GR | GR reading at the interest point, APIU |
| GR _{Clean} | GR average reading in clean section, APIU |
| GR _{Shale} | Average reading 100 % shale section, APIU |
| K_b | bulk modulus |
| L | length |
| P_f | in-situ pore pressure |
| P_{fo} | pore pressure |

| | |
|----------|--|
| P_{ob} | overburden pressure |
| P_w | well pressure |
| S_o | inherent shear strength |
| t | sonic travel time |
| t_c | compression travel time |
| t_f | sonic travel time in pore fluid |
| t_m | compression travel time for matrix |
| T_o | tensile strength of the material |
| t_s | shear travel time |
| t_{sm} | shear travel time for matrix |
| V | volume |
| V_f | compressional-wave velocity of drilling mud |
| V_i | bulk volume factor of each |
| V_s | shear wave velocity |
| V_{sh} | shale volume |
| Z | atomic number (number of electrons per atom) |

CHAPTER 1

INTRODUCTION

Geomechanics is a science which combines solid mechanics, fluid mechanics, engineering, geology and physics. It is used to determine the responses of rocks to force or stress changes.

In the past, geomechanics was not popular among most drilling and production departments. Because of the declined resource volumes and favorable oil prices operators are more eager for drilling deeper and hard well trajectories. Also technological advancements are extending the lives of mature fields. These changes reveal the importance of geomechanics.

There can be severe results for the ones, who do not appreciate the importance of geo-mechanics. Excessive mud loss, wellbore instability (hole enlargement, tight hole, stuck pipe, hole collapse, poor hole cleaning, poor logging, poor cementing), casing compression or shearing, reservoir compaction, surface subsidence, sand production, fault reactivation and loss of reservoir seal are the problems resulting from the stress change. Wellbore stability can be defined as the avoidance of plastic deformation of the rock which surrounds the wellbore. There are four main criteria for wellbore stability analysis;

1. In Situ Stresses (orientation and magnitude)
2. Well Logging (for modeling rock mechanic features),
3. Laboratory Tests (to calibrate rock mechanical modeling),
4. Failure Criteria (Linear Elastic Theory in mechanical stability simulation in terms of failure criterion for the rock) [1].

In these criteria the fourth one which is linear elastic theory eliminates knowledge of in situ stresses, since it is applicable without the knowledge of in situ stresses, also the theory assumes an isotropic, homogeneous, incompressible rock mass, principal stresses are oriented vertically and horizontally, no tectonic forces are acting, the vertical principal stress equals the overburden stress and the rock material is linear elastic.

In this study the purpose is to use geomechanical wellbore stability theory for Sayındere, Karaboğaz, Karababa formations in X field to reveal reliability of Sayındere formation as a casing set place and to show maximum mud weights for this stable formations. For the analysis well log values of X-12 well and core samples from X-11 well are used. The distance between the well is 1064 m and there is not any faults between the wells. For the wellbore stability analysis firstly lithologies of Sayındere, Karaboğaz and Karababa formations are defined with drill cuttings, well log data and X-Ray diffractometer. Then dynamic elastic rock parameters are calculated with gamma ray log, density log and dipole shear sonic imager log. The parameters are also calculated from core samples with laboratory measured density, shear-compressional times and uniaxial compressive strength values. After the calculation of elastic rock parameters, average of maximum mud weights are calculated both from laboratory data and well logs. At the end shear per compressional time values and density values are generalized for these formations.

CHAPTER 2

THEORY

Wellbore stability can be defined as the avoidance of plastic deformation of the rock which surrounds the wellbore. There are four main criteria for wellbore stability analysis;

1. In Situ Stresses (orientation and magnitude)
2. Well Logging (for modeling rock mechanic features),
3. Laboratory Tests (to calibrate rock mechanical modeling),
4. Failure Criteria (Linear Elastic Theory in mechanical stability simulation in terms of failure criterion for the rock) [1].

2.1 In Situ Stresses

2.1.1 Stress in the Subsurface

The stresses acting on a formation can vary in origin, magnitude and direction. Overburden stress equals to in situ vertical stress. Not only vertical stress has a gravitational component but also horizontal stress has a gravitational component may originate from tectonics, thermal effects and geological structure. Moreover, lithology, pore pressure and temperature are stress magnitude and orientation influencing factors. Furthermore rocks ability to respond stress is another important factor.

Shear and normal stresses are main components of force acting on a given area. Normal stress can be defined as a stress which is applied perpendicular to a plane or rock surface and definition for shear stress is the applied stress along

the face of the plane. In terms of the principal axes, one is vertical and one is horizontal, which are orthogonal to each other shear stresses are zero. In situ these orthogonal principal axes are often assumed to be oriented vertically and horizontally (Figure 1). Structural dip of the formation changes the magnitude and orientation of stresses. The orientation of principal stresses can rotate from the vertical and horizontal orientations, due to the presence of faults, salt diapirs, mountains or other complex structures [2].

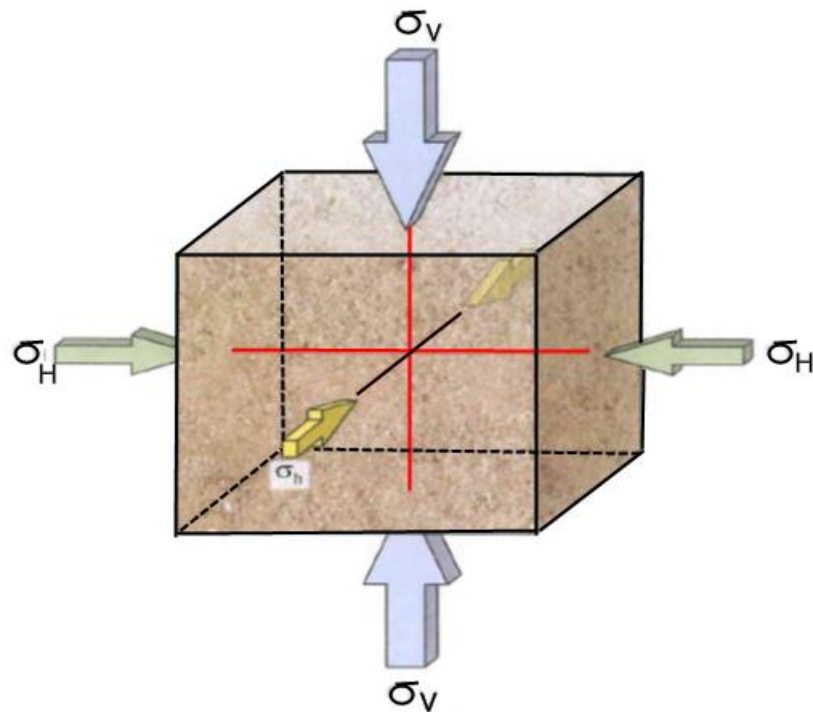


Figure 1 In situ stresses; σ_H for larger horizontal stress, σ_v for vertical stress and σ_h for smaller horizontal stress.

In the earth, the three stress components are linked. Any change of stress in one direction is complemented with the changes in stress along the orthogonal axes. The time when continued deposition brings about greater burial depths, the resulting increase in overburden vertical stress can generate changes in horizontal

stress. This response is generally controlled by the presence of adjacent formations that confine the rock deformation. Differences in formation properties also enforce contrasts in stresses between adjacent lithologies. Furthermore, formation anisotropy can result in greater lateral stress in one direction than in another.

A body of rock responds to applied stress through various modes of strain, causing changes in volume and shape, and rock properties (Figure 2). The spectrum of deformation ranges from reversible to permanent before the failure of the rock. Deformation caused by compression, tension or shear can result in compaction, extension, translation or rotation. Moreover a rock's response to stress depends largely on rock type, cementation, porosity and burial depth. For instance, in limestones, the shape and strength of the skeletal rock framework influence deformation [3].

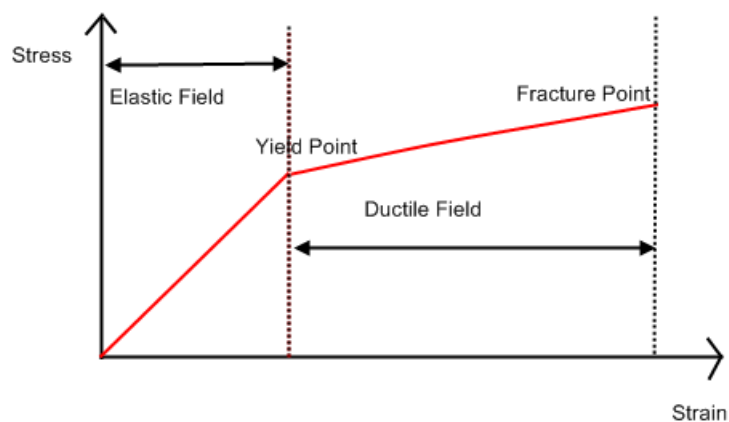


Figure 2 Stress-strain diagram

Small increases in stress generally cause a small deformation. Beyond a certain point, it will deform plastically or fail. The mode of deformation and failure is related with the relationship between changes in maximum and minimum stresses. This relationship is called a stress path.

[4]In petroleum geomechanics, the stress path is the ratio of change in effective minimum horizontal stress to the change in effective overburden stress [5].

2.1.1.1 Vertical Principal Stress

Stresses existing in the subsurface cannot be measured directly [6]. There is main assumption related with the σ_v , as it equals to the overburden stress,

$$\sigma_v = \rho gh$$

Where ρ is overlaying rock mass average density, g for acceleration due to gravity, h is for the depth [7]. Densities of rocks overlaid are used for the calculation of the density which is affected by the change of depth. The values are 0.8-1.0 psi/ft for the range of vertical stress [8].

2.1.1.2 Horizontal Principal Stresses

Hydraulic fracturing is the most used technique for in situ stress calculations [9]. The procedure is pressurizing of rock until the rock fractures. The procedure also necessitates a section is sealed off. Pump is closed when fracture is developed. At the time when fracture closes the pressure is named as P_s , and it decreases firstly fast, than slowly (Figure 3).

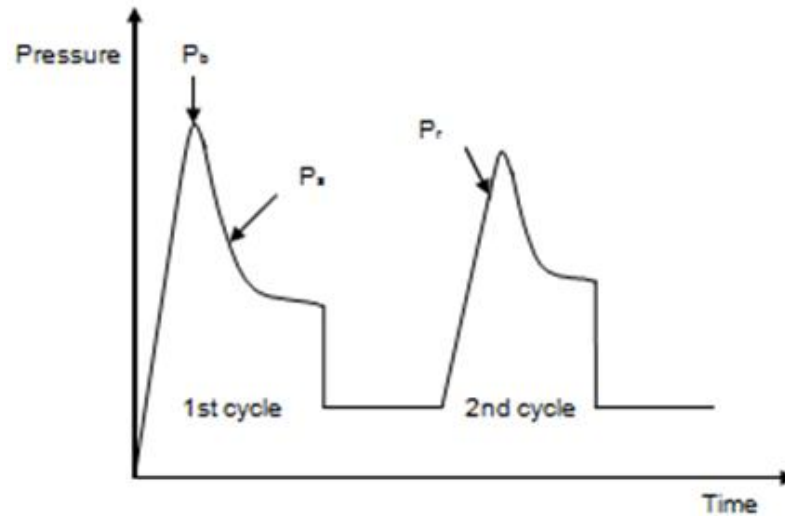


Figure 3 Schematic hydraulic fracturing test

The application is generally applied to vertical boreholes. Furthermore, the necessary assumptions are;

- Wall of the wellbore is not permeable,
- The testes formation is isotropic, meaning that response is independent of stress direction, continuous, meaning that does not have any pre preexisting fractures and formation is linearly elastic.

Leak-off tests (LOTs) are done in deep wells. The procedure is drilling 2-3 meters after the casing shoe. Build up pressure increased until the time when leak off begins. At the LOP wellbore pressure line begins to be not linear. Test is ended at that point. Figure 4 shows a typical leak-off test curve. The LOP is generally taken as the minimum horizontal stress, σ_h . The purpose for the oil industry to do this test is to define the mud pressure in terms of the prevention of fracturing.

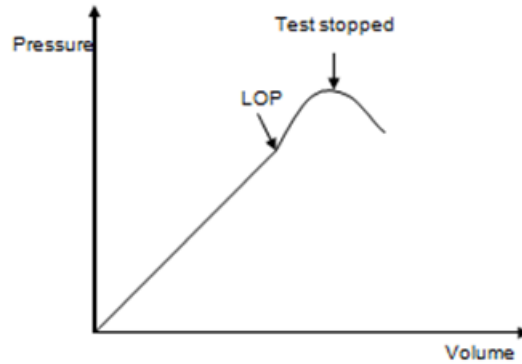


Figure 4 Chart of a leak-off test

Drilling perturbs the in situ stresses and resulting can be breakout or rock yielding. Failure is usually occurring in the way of largest concentration of stress helps to analyze horizontal stress way [10].

$$\sigma_r = P_w$$

$$\sigma_\theta = \sigma_H + \sigma_{\theta h} - 2(\sigma_H - \sigma_{\theta h})\cos 2\theta - P_w$$

$$\sigma_z = \sigma_v - 2\nu(\sigma_H - \sigma_{\theta h})\cos 2\theta$$

Stresses have greatest values at the time $\theta = \pm\pi/2$. Consequently, shear failure initiates in the way of σ_h [1].

2.1.2 Downhole Stressors

To manage reservoirs, oil and gas companies must contend with a variety of downhole stressors-not all of which are caused by over-burden or tectonics. The main downhole stressors can be

1. Pore pressure,
2. Temperature differences,

3. Chemical interactions, which can also affect localized perturbations in stress orientation and magnitude.

2.1.2.1 Pore Pressure

Stress and pore pressure are linked [2]. In formation pore spaces, stress is transmitted to liquids or gases in the form of pressure. The magnitude of pressure applied in any one direction is the same for all directions. If a fluid is compressed, it reacts by exerting an equal and opposite pressure outwards. Under pressure, pore fluids often take up some of the stress imposed on a formation. Temperature is another contributor to the overall stress regime. Temperature differences between drilling fluids and downhole formations will result in heat transfer between the two media. Due to the low thermal conductivity of most rocks, these temperature deviations produce large strain gradients that may result in simple fracturing and realignment of stress. Since thermal expansion of water in the pore space is much higher than that in the rock matrix, the heat transferred into a formation by drilling fluid will generate a larger volume expansion of the pore fluid and a corresponding increase in pore pressure [11].

2.1.2.2 Temperature Differences

Thermal expansion of the rock matrix will generate further stress. A reduction in effective mud support is often associated with an increase in pore pressure. This reduction will lead to a less stable wellbore condition. Conversely, cooling the formation may result in a more stable condition because of decreased pore pressure and tangential stress. The reduction of tangential stress may also lead to a lower hydraulic fracture gradient.

2.1.2.3 Chemical Interactions

Stress and pore pressure can also be affected by interactions between rock and drilling fluid. Shales are particularly sensitive to drilling fluids. Somewhat porous and usually saturated with formation water, these rocks may be susceptible to chemical reactions with certain drilling fluids. When a formation is drilled with an incompatible fluid, the invading filtrate may cause the shale to swell. That may also be susceptible to time dependent changes in effective mud support. They are caused by differences between the mud pressure and pore-fluid pressure. In addition it can be caused by difference between drilling fluid salinity and formation salinity [12]. Furthermore, volume changes in shales arising from interactions between shale and drilling fluid can disturb the stress orientation and magnitude in a borehole.

Local and regional tectonic stresses play a major role in rock deformation. Other downhole factors, such as pore pressure, mud weight and down hole pressure fluctuations, temperature and chemistry also affects local stress-deformation continuum. Their effects may also be tempered by textural properties unique to the local lithology. For instance, the size and distribution of framework grains and pores, mineralogy and the composition of diagenetic cements. It is crucial for an operator to know as much as possible about the rock surrounding a wellbore and the conditions to which it will be subjected.

2.1.3 Changes in Stress

Drilling and production activities affect local stress regimes. Drilling activity perturbs the initial equilibrium of stresses in the near-wellbore region. As a cylindrical volume of rock is excavated through drilling, the stresses formerly exerted on that volume must instead be transferred to the surrounding formation. (Figure 5) This process creates tangential, or hoop stresses, which must be borne by the rock surrounding the borehole. These wellbore stresses are a function of mud weight, wellbore inclination, formation dip angle and azimuth, and the magnitude

and orientation of far-field stresses (σ_v , σ_H , σ_h). Hoop stress varies strongly as a function of borehole radius and azimuth [13].

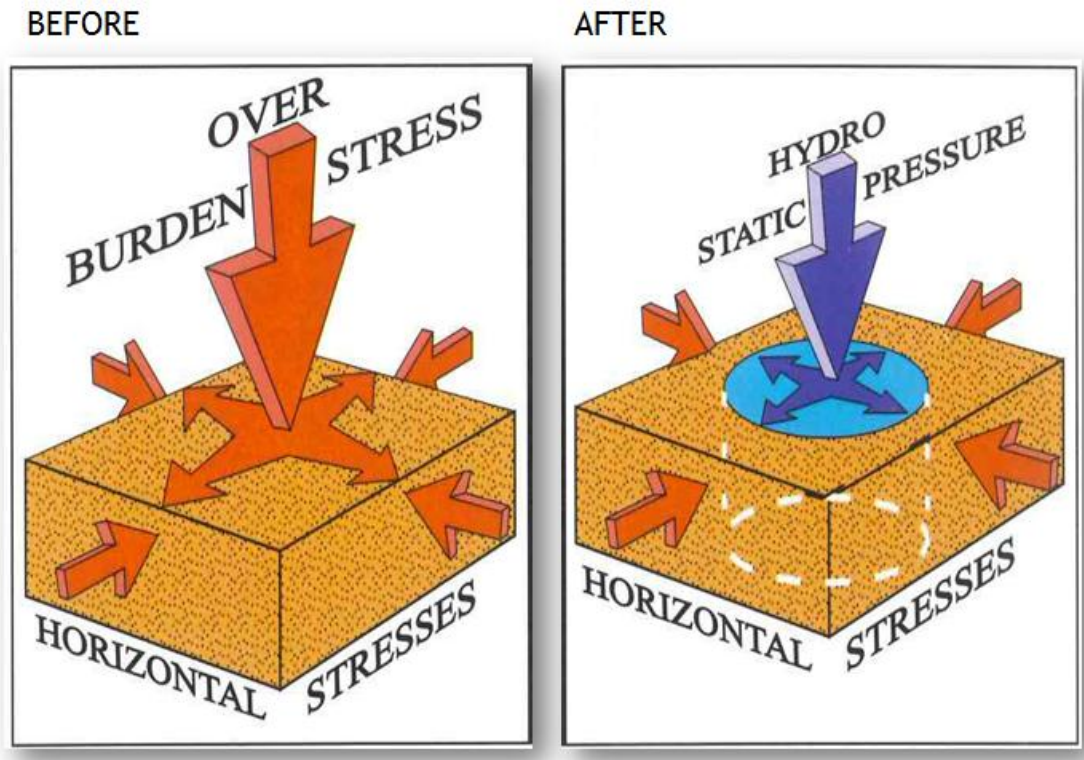


Figure 5 Stresses before and after drilling

In most conventional drilling operations, drillers use hydraulic pressure from drilling fluid as a substitute for the mechanical support that is lost through the cylindrical volume of rock excavated while drilling a wellbore. They essentially replace a cylinder of rock with a cylinder of drilling fluid. However, mud pressure is uniform in all directions, and cannot balance against oriented shear stresses in a formation. As stress is redistributed around the wall of the wellbore, shear stresses can exceed rock strength. When this happens, the wellbore will deform or fail entirely.

Typical examples of geomechanics related drilling problems include wellbore instability and fracturing of the formation. Ramifications include financial loss resulting from lost circulation, kicks, stuck pipe, additional casing strings, sidetracks and even abandonment. To sustain wellbore stability, operators must develop drilling and well construction plans that consider stress magnitude and direction, mud weight, trajectory and pore pressure before, during and after a well is drilled.

Drillers manage pressures imposed by mud weight to avoid wellbore stability problems. Their control of wellbore hydraulics reflects a petroleum engineering approach to a geomechanical problem. During drilling, well-bores can be compromised through a variety of mud-induced modes of failure [14]:

- **Tensile failure** occurs by increasing mud pressure until it causes the wellbore wall to go into tension and eventually to go above the rock's tensile strength. This fractures the rock along a plane at right angles to the direction of minimum stress, often resulting in lost circulation. (Figure 6)

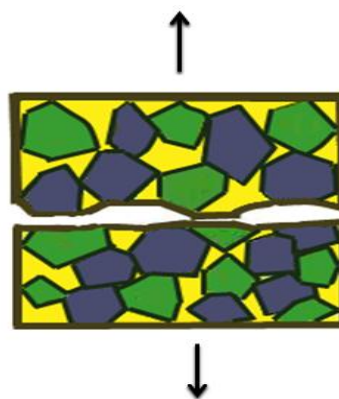


Figure 6 Tensile failure

- **Compressive failure** may be caused by mud weight that is too low or too high. In either case, the formation caves in or spalls off, producing borehole damage and breakouts. Unless the wellbore is properly cleaned out, the accumulation of breakout debris can lead to stuck pipe as the borehole packs off or collapses.
- **Shear displacement** takes place when the mud pressure is high enough to reopen existing fractures that the wellbore has intersected. As a fracture is opened, stresses along the opening are temporarily relieved, allowing opposing faces of the fracture to shear, creating a small but potentially dangerous dislocation along the wellbore.(Figure 7)

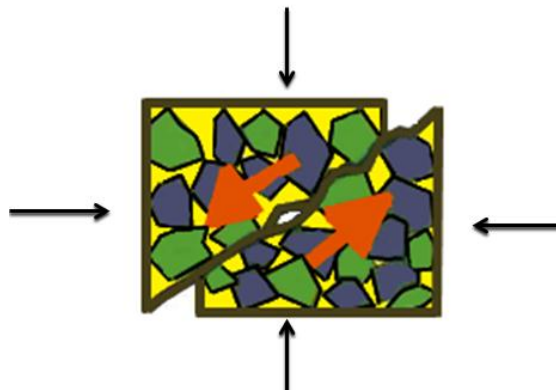


Figure 7 Shear failure

Wellbore stability is further affected by structural factors, such as the interplay between wellbore inclination, formation dip and directional variations in strength between and along formation bedding planes. It is not unusual for some degree of wellbore failure to occur in vertical wells that encounter steeply dipping shales, or inclined wells that intersect shale bedding planes at low angles. Such failures are initiated by low shear and tensile strength along planes of weakness in shales [15].

The issue of strength, or a rock's capacity to withstand stress, points to an important underlying influence on deformation and failure: that of rock fabric [16]. Rock fabric can dictate whether a, given amount of stress will cause a rock to deform or to completely fail, and can influence the extent and orientation of fractures or breakouts in a wellbore. Thus, although borehole breakout is typically assumed to be oriented along the axis of least stress, the bedding, cementation, mineralogy and grain size of a rock may actually redirect the course of a breakout along the rock's weakest points.

For help in anticipating and circumventing problems such as those described above, geomechanics incorporated with well logs, mechanical stability simulation and drilling reports are key solutions.

2.2 Well Logging

For the modeling of rock mechanic features and lithology identification we need well logs namely,

1. Gamma Ray Log,
2. Density Log,
3. Neutron Log,
4. Sonic Log,
5. Dipole Shear Sonic Imager Log.

2.2.1 Gamma Ray (Gr) Log

The GR log is a measurement of the natural radioactivity of the formations. The radioactivity arises from uranium (U), thorium (Th), and potassium (K) present in the rock. The log generally reveals the shale content of the formations in sedimentary formations. The radioactive elements are likely to accumulate in clays and shales. Clean formations generally have a very low level of radioactivity. The GR log can be documented in cased wells as a correlation curve in completion and work over

operations. It is also valuable for position of shales and nonshaly beds and, most outstandingly for general correlation.

Gamma rays are gusts of great energy electromagnetic waves which are discharged spontaneously by some radioactive elements [17]. Approximately all the gamma radiation run into the earth is discharged by the radioactive potassium (K) isotope of atomic weight 40 and by the radioactive elements of the uranium and thorium series.

According to the number and energy of elements they emits the rays [18]. Every collision between the atoms and gamma rays result in loss of energy. Eventually as the gamma ray loses its energy it starts to be absorbed by formation. The effecting factor for the rate of absorption is the density of formation. For instance, two formations with different density values will have dissimilar levels of radioactivity. As the density of formation decreases radioactivity increases. Weight concentration is the main parameter the GR log response:

$$GR = \frac{\sum \rho_i V_i A_i}{\rho_b} \quad (2.1)$$

where

ρ_i : density of each radioactive mineral

V_i : bulk volume factor of each

A_i : proportionality factor of each

ρ_b : bulk density of the formation

The GR log is particularly useful for defining shale beds [17]. The bed boundary is picked at a point midway between the maximum and minimum deflection of the anomaly. Gamma ray deflection increases with shale content of a formation. An

index of the degree of shaliness is obtained by linearly interpolating between the clean level and shale level:

$$\text{Index} = \frac{(\text{GR} - \text{GR}_{\text{Clean}})}{(\text{GR}_{\text{Shale}} - \text{GR}_{\text{Clean}})} \quad (2.2)$$

GR : GR reading at the interest point, APIU

GR_{Clean} : Average reading in clean section, APIU

GR_{Shale} : Average reading 100 % shale section, APIU

The fractional volume of shale, V_{sh} , will be equal to the shale index, I_{sh} , if the density of the formation does not vary with the shale content [19]. This is the situation when thin shale laminations are intermixed with clean sand layers of the same bulk density. The GR log is part of most logging programs in both open and cased hole. [20]

$$V_{\text{sh}} = I_{\text{GR}} \quad (2.3)$$

$$\text{Curve 2 (Older Rocks), } V_{\text{sh}} = 0.333 (2^{2 \cdot I_{\text{GR}}} - 1.0) \quad (2.4)$$

$$\text{Curve 3 (Tertiary Rocks), } V_{\text{sh}} = 0.083 (2^{3.7 \cdot I_{\text{GR}}} - 1.0) \quad (2.5)$$

2.2.2 Density Log

The equation for porosity calculation is:

$$\rho_b = \phi \cdot \rho_f + (1 - \phi) \rho_{ma} \quad (2.6)$$

where ρ_b can be defined as the bulk density, ϕ named as porosity, ρ_{ma} for matrix density, ρ_f for density of pore fluid. For instance sandstone density of matrix 2.65 gm/cc (quartz), limestone density of matrix is 2.71 gm/cc (calcite), dolomite it is about 2.87 gm/cc. The calibration is made for bulk density in grams per cubic centimeter. If there is a "density porosity log", that shows the apparent porosity according to a particular mineral.

2.2.3 Neutron Log

Measurement of apparent porosity units with respect to a given mineralogy is done by neutron logs. The default mineral for calibration is calcite. The values of porosity becomes true porosities in limestone zones. At the places of non-limestone, the limestone-equivalent neutron log must be recalibrated according to the region of matrix mineral. Or else it can be united with density limestone-equivalent porosity in terms of the assessment of the true porosity [20].

2.2.4 Sonic Log

If a sonic log is used for porosity estimation, the equivalent relationship is:

$$\Delta t = \phi \cdot \Delta t_f + (1 - \phi) \Delta t_{ma} \quad (2.8)$$

where Δt is the zone of transit time, Φ for porosity, Δt_{ma} for transit time of the matrix and Δt_f is the transit time for pore fluid. The values for transit times of quartz, calcite and dolomite are 55.5 microseconds per foot, 47.5 microseconds per foot and 43.5 microseconds per foot [20].

2.2.5 Borehole Acoustic Waves

The acoustic waves (Figure 9) recorded by a sonic logging tool depend on the energy source, the path they take and the properties of the formation and the borehole. In wireline logging, there are two primary types of sources, monopole and dipole. A monopole transmitter discharges energy similarly in every direction away from its center. However a dipole transmitter discharges energy in preferred direction.

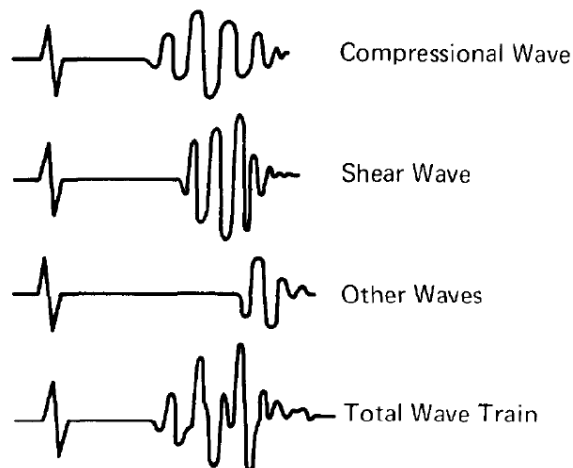


Figure 8 Total wave train and components

From a monopole transmitter located in center of the borehole, a spherical wavefront travels a short distance through the borehole fluid until it meets the borehole wall. Part of the energy is reflected back into the borehole. Rest of the energy causes waves to propagate the formation. The direction of wave propagation is always perpendicular to the wavefront. This simple case also assumes the formation is homogeneous and isotropic, and that the sonic tool itself has no other effect on wave propagation.

In the 2D simplification, when the wavefront in the borehole mud meets the borehole wall, it generates three new wave fronts. A reflected wavefront returns toward the borehole center at speed V_m . Compressional, P-, and shear, S-, waves are transmitted, or refracted, through the interface and travel in the formation at speeds V_p and V_s , respectively. In this simplest case of a hard, or fast, formation, $V_p > V_s > V_m$.

2.2.5.1 P-Waves

A refracted P-wave becomes parallel to the borehole wall, it propagates along the borehole formation interface at speed V_p , faster than the reflected borehole-fluid wave. According to Huygens principle, every point on an interface excited by a P-wave acts as a secondary source of P-waves in the borehole as well as P- and S-waves in the formation. The combination of these secondary waves in the borehole creates a new linear wavefront called a head wave. This first head wave in the mud is known as the compressional head wave, and its arrival at the receivers is recorded as the P arrival. The P-wave takes longer to arrive at receivers that are farther from the source. The time difference between P arrivals divided by the distance traveled is known as Δt , or slowness, and is the reciprocal of speed. This is the most basic sonic-logging measurement.

The P-wave that continues into the formation is known as a body wave, and travels

on deeper into the formation unless a reflector sends it back toward the borehole, at which time it is called a reflected P-wave.

2.2.5.2 S-Waves

The behavior of refracted S-waves is similar to that of refracted P-waves. When the refracted S-wave becomes parallel to the borehole wall, it propagates along the borehole formation interface as a shear disturbance at speed V_s , and generates another head wave in the borehole fluid. Its arrival at the receivers is recorded as the S-wave. In this way, shear slowness of a fast formation can be measured by a tool surrounded by borehole fluid, even though S-waves cannot propagate through the fluid.

In cases when the shear-wave speed is less than the mud-wave speed the shear wavefront in the formation never forms a right angle with the borehole. No shear head wave develops in the fluid in both fast and slow formations, an S body wave continues into the formation.

2.2.5.3 Ray Tracing

Another way of visualizing how P and S head waves and body waves travel near the borehole is through ray tracing. Ray tracing is valid only when the wavelength is much smaller than the diameter of the borehole. Most borehole acoustic modes do not meet these conditions. A ray is simply a line perpendicular to a wavefront, showing the direction of travel. A ray path between two points indicates the fastest travel path.

Ray tracing is useful for understanding where waves travel and for modeling basics of sonic-tool design, such as determining the transmitter-receiver (TR). Ray tracing also helps describe the relationship between TR spacing and near-wellbore altered-

zone thick-ness and velocity contrast. In addition, ray tracing is used in inversion techniques such as tomographic reconstruction.

After the P and S head waves, the next waves to arrive at the receivers from a monopole source are the direct and reflected mud waves. These are followed by trapped modes and interface waves. Trapped modes arise from multiple internal reflections inside the borehole. Wavefronts of particular wavelengths bouncing between the walls of the borehole interfere with each other constructively and produce a series of resonances, or normal modes. Trapped modes are not always seen on logs. They may be affected by borehole condition. In slow formations, trapped modes lose part of their energy to the formation in the form of waves that radiate into the formation. These are called leaky modes, and propagate at speeds between P and S velocities. Leaky modes are dispersive, meaning their different frequency components travel at different speeds.

2.2.5.4 Stoneley Waves

The last arrivals from a monopole source are interface, or surface, waves. A Stoneley wave appears in nearly every Monopole sonic log. Its speed is slower than the shear- and mud-wave speeds, and it is slightly dispersive, so different frequencies propagate at different speeds.

The decay of Stoneley-wave amplitude with distance from the interface is also frequency-dependent. At high frequencies, the amplitude decays rapidly with distance from the borehole wall. At sufficiently low frequencies, the amplitude is nearly constant from one side of the borehole to the other, creating what is known as a tube wave. An example of a tube wave is the water-hammer effect that can sometimes be heard in plumbing pipes when flow is suddenly disrupted.

The low-frequency Stoneley wave is sensitive to formation permeability. When the

wave encounters permeable fractures or formations, the fluid vibrates relative to the solid, causing viscous dissipation in these zones, which attenuates the wave and slows it down. Stoneley-wave dispersion data over a wide bandwidth of frequencies can be inverted to estimate formation permeability [21].

Waveforms recorded at a given depth are initially displayed as a time series from the array of receivers (Figure 9) In some recordings, the P-, S- and Stoneley-wave arrival times can be seen clearly, but often, data-processing techniques are used to pick times accurately. The difference in arrival times divided by the distance between receivers yields the slowness for each mode. However, in many recordings, high noise levels, bad hole conditions or other factors can cause these arrivals to be indistinct or mixed with each other. In such cases, visual or automated picking of arrival times fails to yield true slownesses [22].

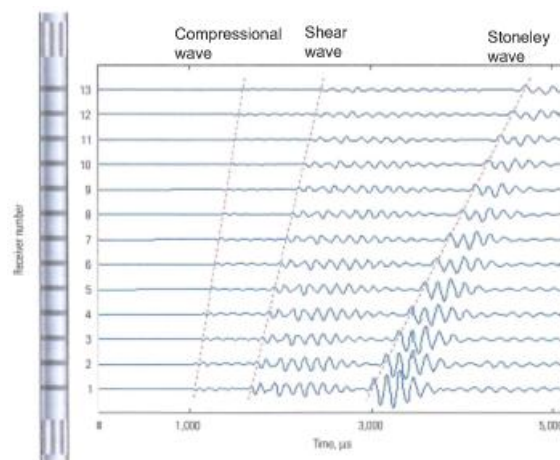


Figure 9 P-waves, S-waves, Stoneley waves.

2.3 Laboratory Tests

The mechanical properties derived from testing rock samples in the laboratory, such as the measurement of the strain for a given applied stress, are static elastic constants.

2.3.1 Core Representativeness, Size Effects, Core Alteration

For the calculation of static rock mechanical parameters cores are needed. Cores can only represent near borehole formations. There will also be always uncertainties due to limited core availabilities. Cores like well logs are taken mostly at the productive zone so there is not any chance for overlying formation interpretations. [8].

The necessary diameter for testing a core sample is 1-2.5". If there exists a inhomogeneity core sample cannot represent all cores. As an example one can consider samples from intact places. Elastic properties changes between fractured place and intact place.

When the core is taken to the laboratory the circumstances are different than in situ. The main differences occur in temperature, stress, fluid contact and pore pressure. Additionally storage conditions, property of handling are other parameters to be think about.

Rock strength is main parameter affecting recovery of cores. When taken to the laboratory mechanical stuffs changes firstly due to the alteration of stress. Horizontal stress may become greater for a time than vertical stress, resulting failure of the rock. The reason behind this is the reduction of vertical stress.

In terms of the ratio consideration the ISRM (International Society for Rock Mechanics) has a 2-3 value standard for the length to diameter ratio. The necessity behind this is the shear plane construction in sideways of core sample [8].

2.4 Linear Elastic Theory

The stress calculations are based on a linear elastic model, which means that the stress-strain curve is linear and strains are completely reversible. The general assumption of linear elasticity is that the components of stress are linear functions of the components of the strain [23]. At the peak stress, total failure takes place. The situation is further complicated by the fact that most rocks do not fail instantly at the peak stress. Strong rocks tend to be more brittle. The brittleness tends to decrease with increasing confining pressure. Weaker rocks are normally more ductile.

In more ductile rocks, plasticity effects should ideally be taken into consideration. More complex models will however require better characterization of the rocks. This is often difficult due to lack of core material. In addition, the rock properties can change significantly over short distances.

Determination of the strength parameters is very much dependent on the availability of core material [24]. This is often limited, and this influences the choice of failure criterion. If the rock can be well characterized, more complex failure criteria can be applied. If not, the choice is limited as Mohr-Coulomb.

2.4.1 The Mohr-Coulomb Criterion

Shear failure occurs when the shear stress along some plane in the sample is too large [8]. Mohr assumed that the failure could be described by:

$$|\tau| = f(\sigma) \quad (2.9)$$

Where σ is the normal stress across a plane and τ is the shear stress along the plane. By choosing specific forms of the function 'f', various failure criteria are obtained. The Mohr-Coulomb criterion assumes a linear 'f'.

$$|\tau| = S_o + \mu\sigma \quad (2.10)$$

Where S_o is the inherent shear strength of the material, where internal friction factor is μ .

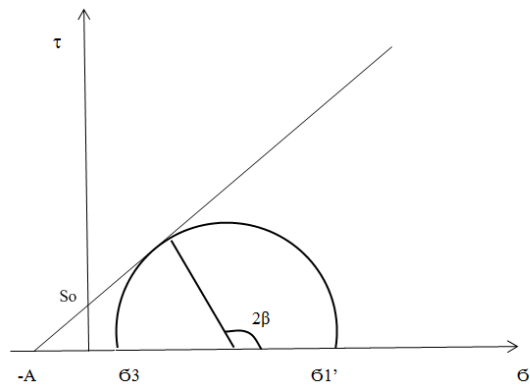


Figure 10 Mohr-Coulomb criterion in τ - σ space.[8]

In Fig. 10 the Mohr-coulomb criterion and a Mohr's circle that touches the failure line were drawn. Here σ_1 is maximum (major) principal stress, σ_3 is minimum (minor) principal stress, β is angle of failure and Φ is angle of internal friction. In the Figure Φ was defined as related to the coefficient of internal friction μ by

$$\tan \Phi = \mu \quad (2.11)$$

It is seen from the Figure that the shear and normal stresses at the point of contact are

$$|\tau| = \frac{1}{2}(\sigma_1 - \sigma_3)\sin 2\beta \quad (2.12)$$

$$\sigma = \frac{1}{2}(\sigma_1 + \sigma_3) + \frac{1}{2}(\sigma_1 - \sigma_3)\cos 2\beta \quad (2.13)$$

And that β and Φ are related by

$$\varphi + \frac{\pi}{2} = 2\beta \quad (2.14)$$

The stresses σ and τ are the normal shear stresses of a plane, the normal of which is inclined at an angle of β to the σ direction. Since the maximum allowable variation of Φ is from 0 to 90° (in practice the range will be smaller, and centred around approximately 30°), it is clear that β will vary between 45° and 90°. Since β is the angle for which the failure criterion is fulfilled, β gives the orientation of the failure plane, and it may be concluded that the failure plane is inclined at an angle smaller than 45° to the σ_1 direction [8].

Introducing the expressions for σ and τ , into the failure criterion, we have

$$\sigma_1 = 2S_0 \tan\beta + \sigma_3 \tan^2\beta \quad (2.15)$$

2.4.2 Uniaxial Compressive Strength

Typical result from a uniaxial test was shown in Fig. 11. The applied stress (σ_z) was plotted as a function of the axial deformation of the sample (ϵ_z). The peak stress is defined as uniaxial compressive strength of the material (C_0). The point beyond which permanent changes will occur is yield point. In elastic region, if the stress is relieved, the specimen will return to its original state. The region in which the sample undergoes permanent deformation without losing the ability to support load is ductile region. In brittle region, the specimens' ability to withstand stress decreases rapidly as deformation increases.

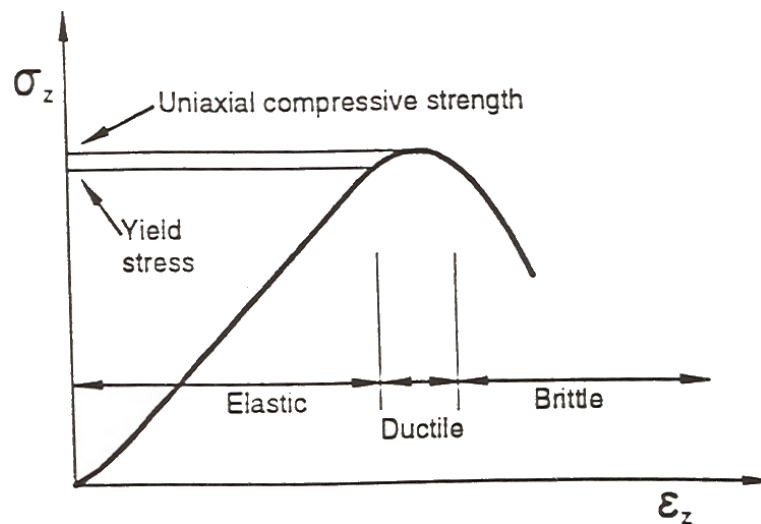


Figure 11 Stress versus deformation in a uniaxial compression test

If the failure mechanism under uniaxial stress is shear failure, uniaxial compressive strength is defined as [8]

$$C_o = 2 S_o \tan\beta \quad (2.16)$$

$$\sigma_1 = C_o + \sigma_3 \tan^2\beta \quad (2.17)$$

CHAPTER 3

3. EXPERIMENTAL SECTION

This chapter consists of two major experiments. These are dynamic elastic rock parameters calculation by well logs and laboratory tests. Well logs used for this calculation are namely gamma ray, density and DSI logs and the laboratory tests are measurements of density, shear times, compressional times and uniaxial compressive strength. Before calculation the homogeneity of formations are checked by analysis of drill cuttings, M-N Plots and XRD analysis.

3.1 Lithology Identification

3.1.1 Drill Cuttings

Cuttings are separated from the drilling fluid when it is circulated out of the hole and across the shale shaker [8]. As a general practice, for every 2 m. interval, samples are looked at and analyzed for visible signs of hydrocarbons and then washed and bagged with a label indicating the depth from which they came. Then, they are further examined by a geologist or mud logger using portable laboratory equipment which can be taken to a well site. Ditch cutting description includes:

- Analysis of clays for sand and silt content,
- Determination of presence of sand and silt,
- Description of the amount of sand/silt,
- Analysis of rock to determine carbonate (limestone/dolomite) content,
- Chemical analysis for rock descriptions,

- Physical tests,
- Oil and gas indications in rock specimens,

There are some problems and factors that must be taken into consideration while making cutting analysis. These are basically cuttings, recirculation, lost circulation material, cement, drilling mud, oil contamination, pipe dope etc. , pipe scale and bit shavings, miscellaneous contaminants, rock dust, powdering, fusing of shales, sample lag time correction, separation of large from small cuttings by relative slippage in the mud. After a well is drilled, cutting analysis is correlated by the well log data. As a result of combination of lithology studies, a guide is obtained for new wells in the area.

3.1.2 M-N Plot

In more complex mineral mixtures, lithology interpretation is facilitated by use of the M-N plot [25]. These plots combine the data of all three porosity logs to provide the lithology dependent quantities M and N. M and N are simply the slopes of the individual lithology lines on the sonic-density and density-neutron cross plot charts. Thus, M and N are essentially independent of porosity, and a crossplot provides lithology identification. M and N are defined as:

$$M = \frac{t_f - t}{\rho_b - \rho_f} * 0.01 \quad (3.1)$$

$$N = \frac{\varphi_{Nf} - \varphi_N}{\rho_b - \rho_f} \quad (3.2)$$

Where t is sonic travel time ($\mu\text{sec}/\text{ft}$), ρ_b is bulk density (gr/cc), φ_N is neutron porosity (limestone units, fractional), and t_f , ρ_f , and φ_{Nf} are the corresponding values of pore fluid. For fresh muds, t_f is $189 \mu\text{sec}/\text{ft}$, ρ_f is $1 \text{ gr}/\text{cc}$, and φ_{Nf} is 1. The multiplier 0.01 is used to make the M values compatible for easy scaling.

If the matrix parameters for a given mineral are used in equations in place of the log values, the M and N values for that mineral are defined. Based on the matrix parameters, M and N values are shown in Table 1 for several minerals in both fresh mud and salt mud filled the holes.

Table 1 Values of M and N for common minerals

| Mineral | Fresh Mud ($\rho_f=1$) | | Salt Mud ($\rho_f=1.1$) | |
|----------------------------------|--------------------------|-------|---------------------------|-------|
| | M | N* | M | N* |
| Sandstone 1 $V_{ma} = 18,000$ | 0.810 | 0.636 | 0.835 | 0.667 |
| Sandstone 2 $V_{ma} = 19,500$ | 0.835 | 0.636 | 0.862 | 0.667 |
| Limestone | 0.827 | 0.585 | 0.854 | 0.621 |
| Dolomite 1 $\phi = 5.5-30 \%$ | 0.778 | 0.489 | 0.800 | 0.517 |
| Dolomite 2 $\phi = 1.5-5 \%$ | 0.778 | 0.500 | 0.800 | 0.528 |
| Dolomite 3 $\phi = 0-1.5 \%$ | 0.778 | 0.513 | 0.800 | 0.542 |
| Anhydrite $\rho_{ma} = 2.98$ | 0.702 | 0.504 | 0.718 | 0.533 |
| Gypsum | 1.015 | 0.296 | 1.064 | 0.320 |
| Salt | | | 1.269 | 1.086 |

* Values of N are computed for CNL neutron log.

Figure 12 is a simplified M-N plot showing the points for several single-mineral formations [17]. The combination selected would depend on the geological probability of its occurrence in the formation.

Secondary porosity and, shaliness, and gas filled porosity will shift the position of the points with respect to their true lithology, and they can even cause M-N points to plot outside the triangular area defined by the primary mineral constituents. The arrows on Figure 8 indicate the direction a point is shifted by the presence of each. In the case of shale, the arrow is illustrative only. The position of shale point will vary with area and formation.

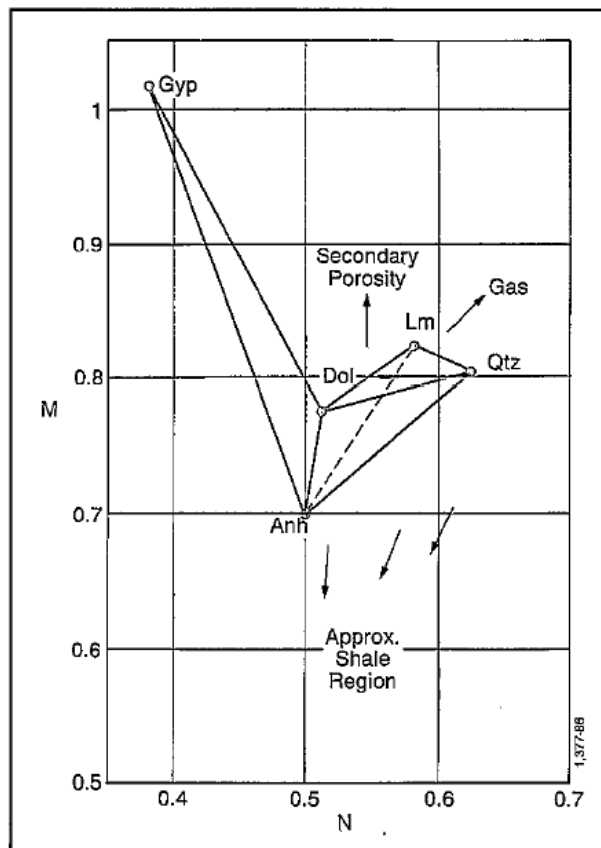


Figure 12 M-N plot for several minerals

In combination with the crossplots using other pairs of porosity logs and lithology sensitive measurements, the M-N plots aid in the choice of the probable lithology.

3.1.3 XRD Analysis

X-Ray Diffraction (XRD) method is simply diffraction of materials by X-ray beams. It diffracts materials according to their atomic pattern. Another definition for X-ray diffraction is taking substance's fingerprint. X-Ray Diffraction Method is a non-destructive tool and brings the analyses of even a small amount of sample. For instance, the qualitative and semi-quantifiable studies of rocks, crystalline materials, thin films and polymers can be performed by X-Ray Diffractometer (Figure 13) [26].



Figure 13 X Ray Diffractometer [26]

3.2 Dynamic Elastic Properties

Poisson's Ratio, Shear Modulus, Young's Modulus, Bulk Modulus, Bulk Compressibility and Rock Compressibility are dynamic elastic properties obtained from acoustic log measurements with density log assuming an infinite, isotropic, homogeneous and elastic medium.

Dynamic elastic constants are derived from the measurement of borehole acoustic waves in the material. Sonic logging and waveform analysis provide the mean for obtaining continuous measurements of compressional and shear velocities.

Consider a sample of length L and cross-sectional area $A = D^2$. When the force F is applied on its end surfaces, the length of the sample is reduced to L' . The applied stress is then $\sigma_x = F/A$ and the corresponding elongation is $\epsilon_x = (L - L')/L$. If the sample behaves linearly there is a linear relation between σ_x and ϵ_x , which can be written as

$$\epsilon_x = \frac{1}{E} \sigma_x \quad (3.3)$$

Equation is known as Hooke's law, while the coefficient E is called Young's modulus. Young's Modulus is a measure of stiffness of the sample, the sample's resistance against being compressed by a uniaxial stress.

Another consequence of applied stress σ_x is an increase in the width D of the sample. The lateral elongation is $\epsilon_y = \epsilon_z = (D - D')/D$. In general $D' > D$, thus ϵ_y and ϵ_z become negative. The ratio is defined as Poisson's ratio. It is a measure of lateral expansion relative to longitudinal contraction.

$$\nu = -\frac{\epsilon_y}{\epsilon_x} \quad (3.4)$$

Another elastic parameter is shear modulus, G, also known as modulus of rigidity, which is a measure of sample's resistance against shear deformation. Yet another important elastic modulus is bulk modulus, K, defined as ratio of hydrostatic stress $\bar{\sigma}_p$ relative to volumetric strain ϵ_{vol} . It is a measure of the sample's resistance against hydrostatic compression. The inverse of K is, i.e 1/K, is known as the compressibility. The value of "a" in Table 2 is used as $1,34 \times 10^{10}$ when density is in gr/cc and times are in $\mu\text{sec/ft}$ [8].

Table 2 Elastic rock parameters

| | | |
|---|--|---|
| POISSON'S RATIO ,ν | $\frac{\text{Lateral Strain}}{\text{Longitudinal strain}}$ | $\frac{0,5 * \left(\frac{ts}{tc}\right)^2 - 1}{\left(\frac{ts}{tc}\right)^2 - 1}$ |
| SHEAR MODULUS ,G | $\frac{\text{Applied stress}}{\text{Shear strain}}$ | $\frac{\rho b * a}{ts^2}$ |
| YOUNG'S MODULUS ,E | $\frac{\text{Applied uniaxial stress}}{\text{Normal strain}}$ | $2 * G * (1 + \nu)$ |
| BULK MODULUS ,K_b | $\frac{\text{Hydrostatic pressure}}{\text{Volumetric strain}}$ | $\rho b \left[\frac{1}{tc^2} - \frac{4}{3ts^2} \right] * a$ |
| BULK COMPRESSIBILITY (with porosity) ,c_b | $\frac{\text{Volumetric deformation}}{\text{Hydrostatic pressure}}$ | $\frac{1}{K_b}$ |
| BULK COMPRESSIBILITY (zero porosity) ,c_r | $\frac{\text{Change in matrix volume}}{\text{Hydrostatic pressure}}$ | $\frac{1}{\rho_g \left[\frac{1}{tma^2} - \frac{4}{3tma^2} \right] * a}$ |

Acoustic wave propagation properties of rocks are known to depend on porosity, rock matrix composition, stress (overburden and pore fluid pressure), temperature, fluid composition, and texture (structural framework of grains and-pore spaces).

With the combination of dynamic elastic constants with inputs of pore pressure, overburden pressure, and mud weight allows the stresses within the formation and around the borehole to be computed.

3.3 Laboratory Tests

The mechanical properties derived from testing rock samples in the laboratory, such as the measurement of the strain for a given applied stress, are static elastic constants.

For the calibration of the rock mechanical modeling we need core based laboratory tests namely,

1. Specific Gravity Measurement by Pycnometer,
2. Shear and Compressional Time Measurement by Sonic Viewer,
3. Uniaxial Compressive Strength Measurement,

3.3.1 Specific Gravity Measurement

The density, ρ , is a physical property. The definition for a uniform body is ratio of mass m to volume V .

$$\rho = \frac{m}{V} \quad (3.5)$$

The SI unit for the density it is kg/m^3 . Still, g/cm^3 is generally used. The equivalency between them is

$$1 \frac{\text{g}}{\text{cm}^3} = 1000 \frac{\text{kg}}{\text{m}^3} \quad (3.6)$$

In terms of the volumetric thermal expansion of rock the volume of an object rises with growing temperature. As the temperature increases volume is increases the result is decrease in density value. One of exclusion is water. For the range of temperature 0-4 °C, the density increases with increasing temperature. Furthermore, gas densities are related with pressure applied. This result is insignificant in a circumstance of liquid or solid matter [27].

3.3.2 Density determination of solid matter by Pycnometer

Pycnometer (Figure 14, 15) may used to define the density of uniform solid body which is not dissolving in working liquid (water). The first step is the measurement of the weight of object and Pycnometer as m_0+m_s . To do this water is added to define the weight m_{H_2O} (measured weight minus m_0+m_s). So the volume of added water V_{H_2O} may be found as

$$V_{H_2O} = \frac{m_{H_2O}}{\rho_{H_2O}} \quad (3.7)$$

The difference between the volume of water that fills the empty pycnometer V and volume V_{H_2O} is the volume of measured solid body V_s is [27].

$$V_s = V - V_{H_2O} = \frac{m_{H_2O} - m'_{H_2O}}{\rho_{H_2O}} \quad (3.8)$$

The value of object density ρ_s becomes;

$$\rho_s = \frac{m_s}{V_s} \quad (3.9)$$



Figure 14 Pycnometer

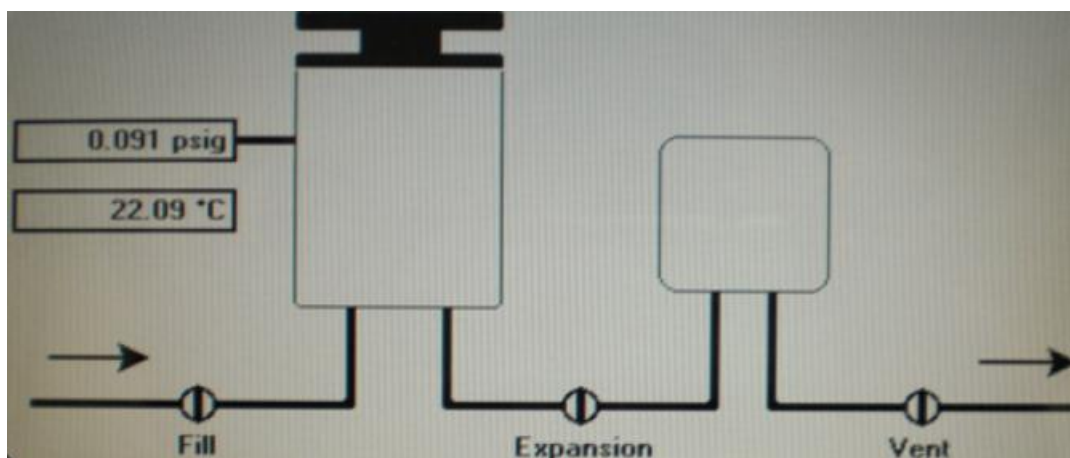


Figure 15 Experimental set-up

3.3.3 Shear and Compressional Time Measurement by Sonic Viewer

Acoustic anisotropy is also related with cracks due to the sensitiveness of acoustic wave velocities and attenuations. This anisotropy is conserved when the core has entered the laboratory. The measurements of it may help as additional information to calculate in situ principal stress directions.

Caution must be taken in advance a directional velocity deviation is interpreted as anisotropy. The reason behind this deviation may due to the inhomogeneties.

3.3.3.1 Ultrasonic Velocity Measuring System for Rock Sample

The SonicViewer-SX (Figure 16) is an instrument for the ultrasonic wave velocity measurement of rock samples. It is possible to read the P and S wave propagation with high accuracy, because it contains high voltage (500V) pulser and receiver which consists of 10 bit, 50nsec A to D converter. In addition, input of the parameter of length and density of the rock sample previously, then it can calculate dynamic poisson's ratio and dynamic shear modulus by built in software [28].



Figure 16 Sonic viewer [28]

3.3.4 Uniaxial Compressive Strength Measurement

One of the ways for uniaxial compressive strength measurement is the unconfined compression test. For this test a core sample is put in into a load frame. Then by increasing the axial load with zero confining pressure the test is done. The test can also be seen as a triaxial compression test simplification. The measurable parameters at the end of the test are:

- The unconfined compressive strength C_o as the greatest stress.
- Young's modulus which is E_{fr} ,
- Poisson's ratio ν_{fr} which can be taken as the ratio between radial and the axial strain.



Figure 17 Uniaxial compressive strength test machine

Most rocks exhibit brittle failure in unconfined failure tests, so it is straightforward to identify ν .

In case of anisotropic rock mass, the values of Poisson's ratio and Young's Modulus are not appropriate factors to define the mechanical behavior. Value of the measured Poisson's Ratio be governed by both on the route of load that applied and the route of lateral strain measurement. Consequently there should be a specification for the orientation of the sample's symmetry regarding the directions of applied and measured stress and strains.

In theory, one of the important factor for the measurement of the uniaxial compressive strength is presence of cracks. Therefore it is important in terms of coring and handling not to cause cracks. As a result uncertainties can occur in terms of the testing of weak rocks.

3.4 Borehole Failure Criteria

Stress differences may occur when P_w is different than the P_f . When stress is exceeds rocks strain limit then borehole failure occurs. In the condition of the stress deviance in someplace go above the failure criterion for the rock, the rock failure occurs [24]. The situation is known as "borehole failure" does not have the meaning of lost well.

3.4.1 Vertical, Impermeable Borehole in a Linear Elastic Formation (with no porosity)

Linear elastic materials which responds as elastic, i.e. the stress-strain curve is linear and strains are completely reversible, the biggest stress difference occur at the

borehole wall, since failure of the rock begins to form there [8]. Principal stresses for a vertical borehole in a formation with isotropic horizontal stress are,

$$\sigma_r = P_w \quad (3.10)$$

$$\sigma_\theta = 2 \sigma_h - P_w \quad (3.11)$$

$$\sigma_z = \sigma_v \quad (3.12)$$

$$\sigma_h = \frac{\nu}{(1-\nu)} (P_{ob} - P_f) + P_f \quad (3.13)$$

$$P_{ob} = \int_0^D \rho(D) g dD \quad (3.14)$$

where P_w is well pressure and, P_f is formation pressure, σ_v is vertical stress, σ_h is horizontal stress, P_{ob} is overburden pressure, D is depth and $\rho(D)$ is the density of overburden at depth D , and 'g' is acceleration of gravity.

3.4.1.1 Shear failure

“Borehole failure” can occur, depending on the relative magnitude between the “principal stresses”. When the condition is $\sigma_\theta > \sigma_z > \sigma_r$ at the borehole wall, Mohr-Coulomb criterion failure happens;

$$\sigma_\theta = C_o + \sigma_r \tan^2 \beta \quad (3.15)$$

$$C_o = \frac{2 \cos \varphi}{1 - \sin \varphi} \times \frac{0.026E}{cb \cdot 10^6} [0.008V_{clay} + 0.0045(1 - V_{clay})] \quad (3.16)$$

$$\beta = \frac{\pi}{4} + \frac{\varphi}{2} \quad (3.17)$$

where β can be defined as angle of failure in between the failure plane normal and major of principal stress axis. C_o is uniaxial compressive strength, E is Young's modulus, c_b is bulk compressibility, Φ is friction angle and taken as 30° in general. Introducing the expression for σ_θ and σ_r into Eq. the result for well pressure turns into;

$$P_w = \frac{2\sigma h - C_o}{\tan^2 \beta + 1} \quad (3.18)$$

Therefore, the time when P_w falls below the value given by Eq. shear failure starts to occur at the wellbore wall.

With the assumption of P_w is increased, so that $\sigma_r > \sigma_z > \sigma_\theta$, the Mohr-Coulomb criterion predicts failure when

$$\sigma_r = C_o + \sigma_\theta \tan^2 \beta \quad (3.19)$$

$$P_w = \frac{2\sigma h \tan^2 \beta + C_o}{\tan^2 \beta + 1} \quad (3.20)$$

This criterion states that shear failure forms at the wall of the borehole gets a value bigger than that found by the Eq. Thus, there are both an upper and a lower limit for the well pressure, forming a region that in terms of the shear failure borehole is stable. If there is a large difference between the horizontal and the vertical stresses, the failure criterion may be fulfilled already when σ_z is still the largest (or alternatively the smallest) principal stress. Since in terms of the definition of stable region there is a need to permute the six conditions of principal stresses σ_r , σ_θ and σ_z .

3.4.1.2 Tensile failure

In addition, σ_θ value can be negative when the well pressure is sufficiently large. If $\sigma_\theta < -T_o$, where T_o is the tensile strength of the material, the failure occurring at the wellbore all is tensile failure. The resulting criterion in terms of the failure is:

$$P_w = 2\sigma_h + T_o \quad (3.21)$$

The condition says that tensile failure begins forming at the borehole wall if the P_w has a greater value than the result calculated by Eq. The name of such failure is “hydraulic fracturing”.

3.4.2 Vertical, Impermeable Borehole in a Linear Elastic Formation (with porosity)

3.4.2.1 Shear Failure

In a field situation, the rock surrounding the borehole is normally porous and permeable [8]. Hence, the pore pressure has to be included in the failure criterion for the borehole. This can be done by applying a failure criterion for poroelastic materials, like the Mohr-Coulomb criterion.. Conditions for shear failure in boreholes with impermeable borehole wall [8].

$$\text{Case 'a'} \quad \sigma_\theta \geq \sigma_z \geq \sigma_r \quad P_w \leq P_f + \frac{2(\sigma_h - P_f) - C_o}{\tan^2 \beta + 1} \quad (3.22)$$

$$\text{Case 'b' } \sigma_z \geq \sigma_\theta \geq \sigma_r \quad P_w \leq P_f + \frac{[\sigma_v - P_f - C_o]}{\tan^2 \beta} \quad (3.23)$$

$$\text{Case 'c' } \sigma_z \geq \sigma_r \geq \sigma_\theta \quad P_w \geq P_f + 2(\sigma_h - P_f) - \frac{[\sigma_v - P_f - C_o]}{\tan^2 \beta} \quad (3.24)$$

$$\text{Case 'd' } \sigma_r \geq \sigma_z \geq \sigma_\theta \quad P_w \geq P_f + \frac{2(\sigma_h - P_f) \tan^2 \beta + C_o}{\tan^2 \beta + 1} \quad (3.25)$$

$$\text{Case 'e' } \sigma_r \geq \sigma_\theta \geq \sigma_z \quad P_w \geq P_f + (\sigma_v - P_f) \tan^2 \beta + C_o \quad (3.26)$$

$$\text{Case 'f' } \sigma_\theta \geq \sigma_r \geq \sigma_z \quad P_w \leq P_f + 2(\sigma_h - P_f) - (\sigma_v - P_f) \tan^2 \beta - C_o \quad (3.27)$$

If the borehole is vertical, the horizontal stress is isotropic and for impermeable borehole wall, the stresses at the borehole wall are given by Eqs. Substitution of the principal stresses σ_z , σ_θ , and σ_r from Eqs. into the failure criterion may be done in six different ways, in terms of the relative magnitudes of the stresses.

3.4.2.2 Tensile failure

Tensile failure may occur if P_w becomes large to make σ_θ negative. The criterion for tensile failure for a proelastic material is

$$\sigma_\theta' < -T_o \quad (3.28)$$

Tensile failure happens the time when P_w is bigger than below Eq.

$$P_w = 2\sigma_h - P_f + T_o \quad (3.29)$$

There also exists one more failure criterion. If there is a pre-existing fracture in the borehole wall, vertical component of pressure applies a force on the formation there [8]. A horizontal fracture will then grow if $(\sigma_v - P_w)$ is less than $(-T_o)$, i.e. if $P_w > \sigma_v + T_o$.

3.4.3 Permeable Borehole

P_f equals P_w when the borehole is permeable. In a steady state situation, the borehole failure criterion corresponding to case 'a' becomes:

$$P_w = \frac{2\sigma_h - C_o - \alpha P_{fo} \frac{1 - 2\nu}{1 - \nu}}{1 + \alpha + (1 - \alpha) \tan^2 \beta - \alpha \frac{1 - 2\nu}{1 - \nu}} \quad (3.30)$$

The criterion coincides with the criterion 'a', if $P_w = P_f = P_{fo}$, where P_{fo} is in-situ pore pressure. This is close to the situation normally occurring during drilling, where the well pressure is kept slightly above the pore pressure.

Also, the criterion is based on the assumption that the pore pressure gradient is stable (i.e. steady state), and that it may take a long time before this requirement is met. The effect of a non-stable pore pressure gradient can be modeled qualitatively by a modification of the in situ pore pressure P_{fo} in Eq. if the well pressure is changed ΔP_w from a steady state situation, the effective in situ pore pressure in Eq. becomes

$(P_{fo} + \Delta P_{fo})$, where ΔP_{fo} is proportional to $-\Delta P_w$, and decays with time. Thus, the failure criterion changes with the time, due to the change in the pore pressure gradient.

3.4.4 Effect of Non-linearity

The criterion for borehole failure described is often found to give pessimistic estimates of the borehole strength. In some cases, these criteria may have been exceeded by several hundred per cent before the borehole fails [29]. A possible explanation for this may be that the stress solutions used to obtain these criteria are not valid in the vicinity of the borehole, due to non-linear effects.

The stress state near the borehole is significantly altered, if the Young's modulus of the rock is stress dependent. In particular, it was shown that for low well pressures, the tangential stress may be largely reduced in the surrounding area of the wellbore [8]. This implies that the borehole can take much lower well pressures before it fails, as compared to a borehole in a formation with constant elastic moduli. This effect is due to the low Young's modulus of the rock close to the borehole wall, caused by the low radial stress in this region. Thus, there is a region close to the borehole where the rock can take large deformations without correspondingly large stress concentrations. This region is effectively shielding the outer part of the formation against the low radial stress at the borehole wall.

3.4.5 Evaluation of Input Data

Evaluation of input data is very important in a stability analysis [8]. However, very often the knowledge of these is insufficient. Hence the uncertainty in the results increases. The complexity in the stress situation makes it difficult to make general comments about the effect of the various stress components. Effective stresses are

controlled by the pore pressure. It is the effective stresses which control both compressive and tensile failure. In the permeable reservoir section the pore pressure can be measured with reasonable accuracy. However, in the low-permeable shale sections above the reservoir, direct measurements of the pore pressure are not possible. Pore pressure prediction is then based on other parameters (e.g. drilling parameters or logging parameters) and their deviation from normal trend lines. Detection of abnormally pressured shale sections may however be difficult, and failure to detect these zones may result in stability problems. If the well pressure is lower than the pore pressure (drilling underbalanced), a zone of tensile radial stress will exist near the wellbore.

If the tensile radial stress exceeds the tensile strength of the rock, spalling will occur [8]. A new free surface will be exposed to exactly the same effect; hence this is a process which is not self-stabilizing.

CHAPTER 4

STATEMENT OF PROBLEM

Wellbore stability problems during drilling cause substantial problems in all areas of the world. These stability problems are often resulting in loss of time and sometimes loss of equipment. According to Amoco wellbore stability related problems may amount up to 17 % of the total drilling budget of a well. So it is important to prevent the stability related wellbore problems.

In this study geomechanical wellbore stability is analyzed for X production field in Southeastern Anatolia for the productive zone formations namely; Sayındere, Karaboğaz and Karababa to reveal reliability of Sayındere formation as a casing set place and to show minimum and maximum mud weights for these formations. The used geomechanical wellbore stability assessment needs stress-strain relationships. To analyze the studied formations rock properties their elastic constants' determined from a specimen of the rock under load in a testing machine in combination with pycnometer measured densities; referred as the static elastic constants. Moreover, dynamic elastic constants also determined, using wave-propagation relationships in combination with bulk density, referred as the dynamic elastic constants. By the use of linear elastic theory and calculated rock properties, minimum and maximum mud weights determined to define the mud weight window which is the main parameter for wellbore stability.

Final purpose is to generalize shear and compressional time values and densities for studied formations. By the use of generalized values it possible to calculate the rock strength parameters for studied formations drilled in Southeastern Anatolia, without recording DSI and FDC-CNL logs.

CHAPTER 5

RESULTS AND DISCUSSION

In this study the purpose is to use geomechanical wellbore stability theory for Sayındere, Karaboğaz, Karababa formations in X field to reveal reliability of Sayındere formation as a casing set place and to show maximum mud weights for this stable formations.

5.1 Well Information

The related production field is located in Adıyaman, Turkey and discovered 2006. There are 13 wells drilled in the field.

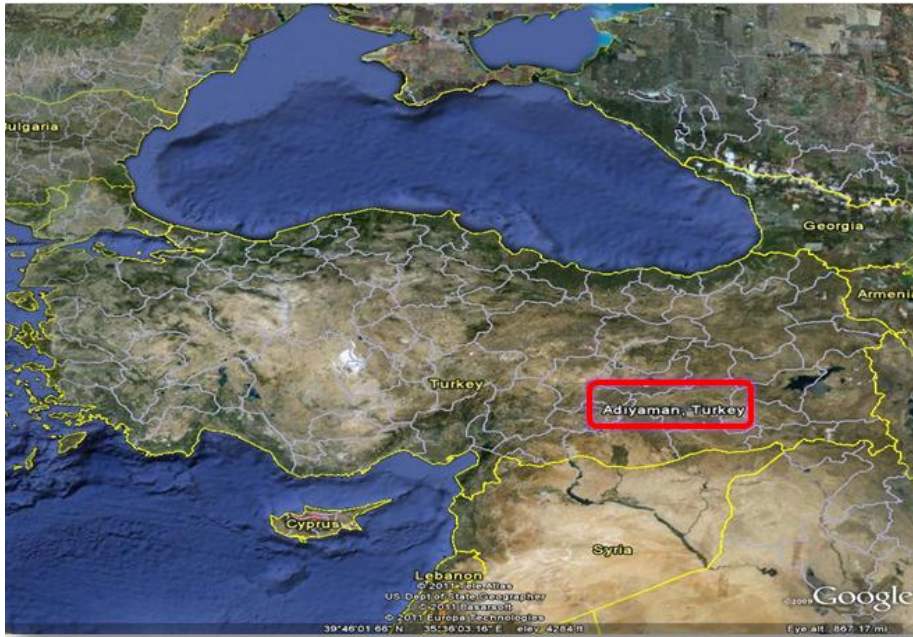


Figure 17 Field location in map

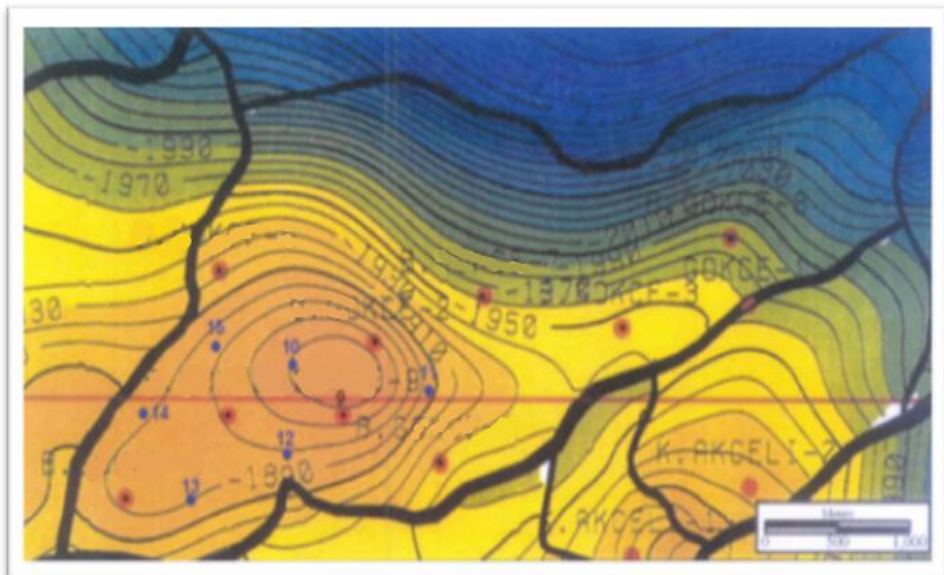


Figure 18 Well locations [29]

Field is homogeneous and there is not any fault between the wells. For the analysis the well log data of X-12 and core samples from X-11 are used. The distance between these two wells is 1064 m.

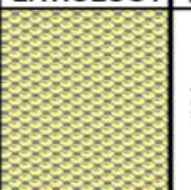

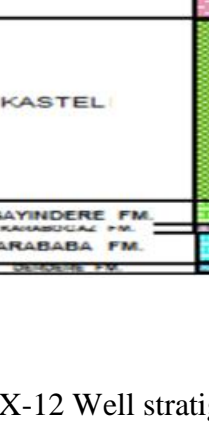



| AGE | FORMATION | LITHOLOGY | DEPTH |
|------------------|---------------|---|--------|
| UPPER MIOCENE | ŞELMO |  | 584 |
| | | | 584 m |
| EOCENE | MIDYAT |  | 438 |
| | | | 1022 m |
| PALEOCENE | GERMAV |  | 920 |
| | | | 1942 m |
| UPPER CRETACEOUS | KASTEL |  | 562 |
| | | | 2504 m |
| | SAYINDERE FM. |  | 2612 m |
| | KARABABA FM. |  | 2662 m |

Figure 19 X-12 Well stratigraphic column [29]

In the field the conductor casings (13 3/8") are set to the Şelmo formation, intermediate casings (9 5/8") are set at the beginning of Sayındere formation and finally production casings (7") are set to the final depth. The formations having

problem are Germav and Kastel. These formations are drilled within 12 ¼” hole section and this section needs mud weights from 68 ppcf to 82 ppcf. The studied formations are drilled with a mud weight of 66-68 ppcf without having any stability problem.

5.2 Formation Information and Lithology Identification

5.2.1 Formation Information

5.2.1.1 Sayındere Formation

Formation is a member of Adıyaman Group and first defined by Gossage in 1959 at 10 km west of Gölbaşı as Lower part of Germav group in Sayındere platy limestone formation. Age is Upper Campanien.

5.2.1.2 Karaboğaz Formation

Formation is a member of Adıyaman Group. Formation outcrop is seen at 32 km south of Adıyaman at south side of Mount Karababa. Age is Middle Campanien. Formation is drilled most of wells in Southeastern Anatolia at thicknesses of 10-60 m.

5.2.1.3 Karababa Formation

Karababa formation belongs to the Mardin group. Formation outcrop can be seen at 32 km south of Adıyaman, at north of Fırat valley which is located in south of mount Karababa. The formation is composed of three members namely Karababa A, B and C members. The first definition for the formation is made by Gossage in 1956. Age for the formation is Campanien. [30].

5.2.2 Lithology Information

Lithology identification was made by using drill cuttings, well logs and X-Ray Diffractometer mineral analysis report.

| INTERVAL | LITHOLOGY |
|---|--------------------|
| KASTEL / SAYINDERE LD. 2504 m (-1773.70) | |
| 2504-2524 | LIMESTONE |
| 2524-2560 | LIMESTONE |
| 2542-2560 | LIMESTONE |
| 2560-2598 | LIMESTONE |
| 2598-2612 | LIMESTONE |
| SAYINDERE FM / KARABOĞAZ FM L.D. 2612 m (-1881.70) | |
| 2612-2628 | LIMESTONE |
| | CHERT |
| 2628-2634 | LIMESTONE CHERT |
| 2634-2638 | LIMESTONE |
| 2638-2640 | LIMESTONE |
| | CHERT |
| 2640-2642 | LIMESTONE |
| KARABOĞAZ FM / KARABABA-B FM F.D. 2642 m (1911.70) | |
| 2642-2650 | LIMESTONE |
| | CHERT |
| 2650-2658 | LIMESTONE |
| 2658-2660 | LIMESTONE |
| KARABABA B FM / KARABABA A FM L.D. 2662 m (-1931.70) | |
| 2662-2666 | LIMESTONE |

Figure 20 Drill cuttings report [29]

According to the drill cuttings (Figure 20) Sayindere formation is composed of limestone and Karaboğaz formation is composed of limestone and chert and Karababa formation is composed of mostly limestone and with a few chert.

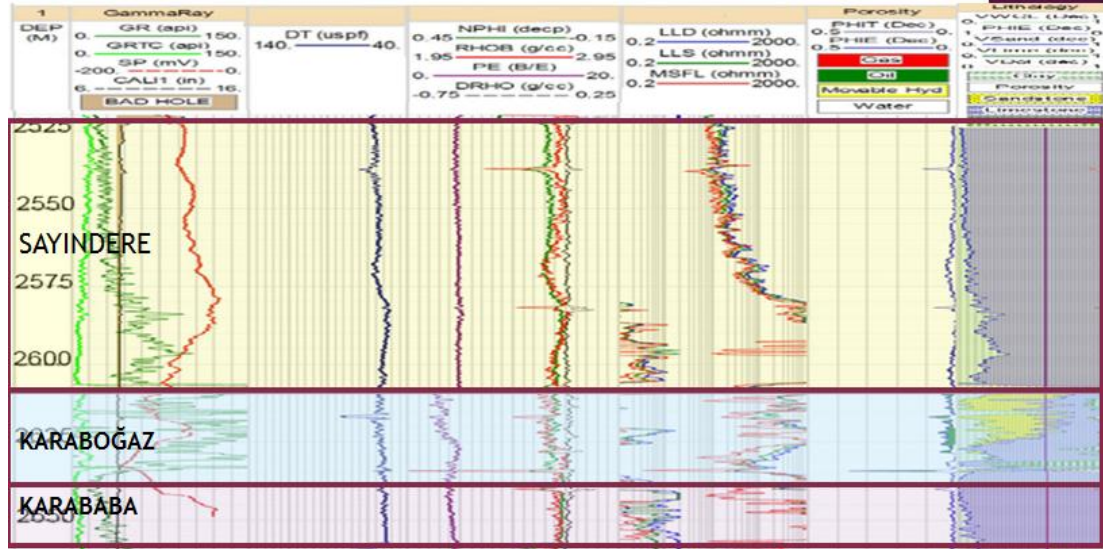


Figure 21 Available Well Logs for X-12 Well [29]

The results of well logs (Figure 21) also support the lithology identified by drill cuttings. The logs are taken by 1 m interval. And M-N plot analysis made to show the parallelism.

$$M = \frac{t_f - t}{\rho_b - \rho_f} * 0.01 \quad (5.1)$$

$$N = \frac{\varphi_{Nf} - \varphi_N}{\rho_b - \rho_f} \quad (5.2)$$

According to the equations shown, M and N values are calculated and the results are presented in Figure 22, Figure 23, Figure 24 for Sayındere, Karaboğaz and Karababa formations. The calculated values from well logs, drill cuttings are also supported by the XRD (X-Ray Diffractometer) (Table 3). The analysis is made from the core samples taken from X-11 well, and results are in consistency with other analysis. According to the results Karaboğaz has heterogeneous mineralogical content such that the composition may form from quartz and calcite or it may calcite and dolomite. This content change also explains the deviations of gamma ray line for this formation.

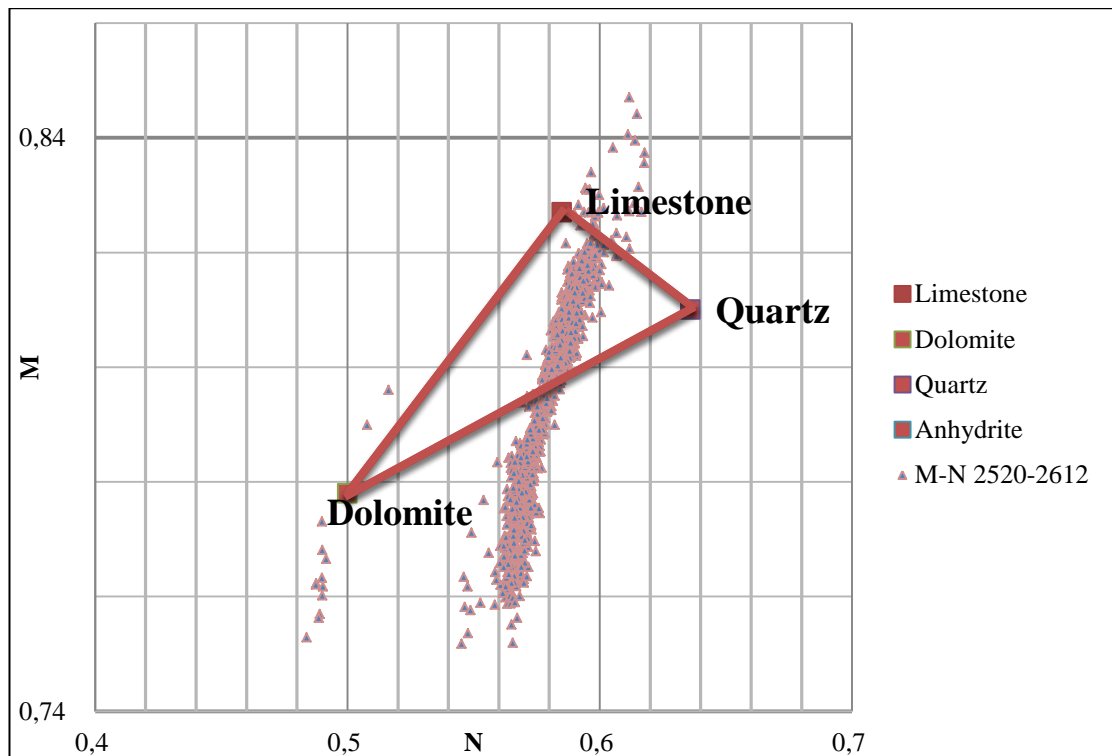


Figure 22 M-N plot for Sayındere formation

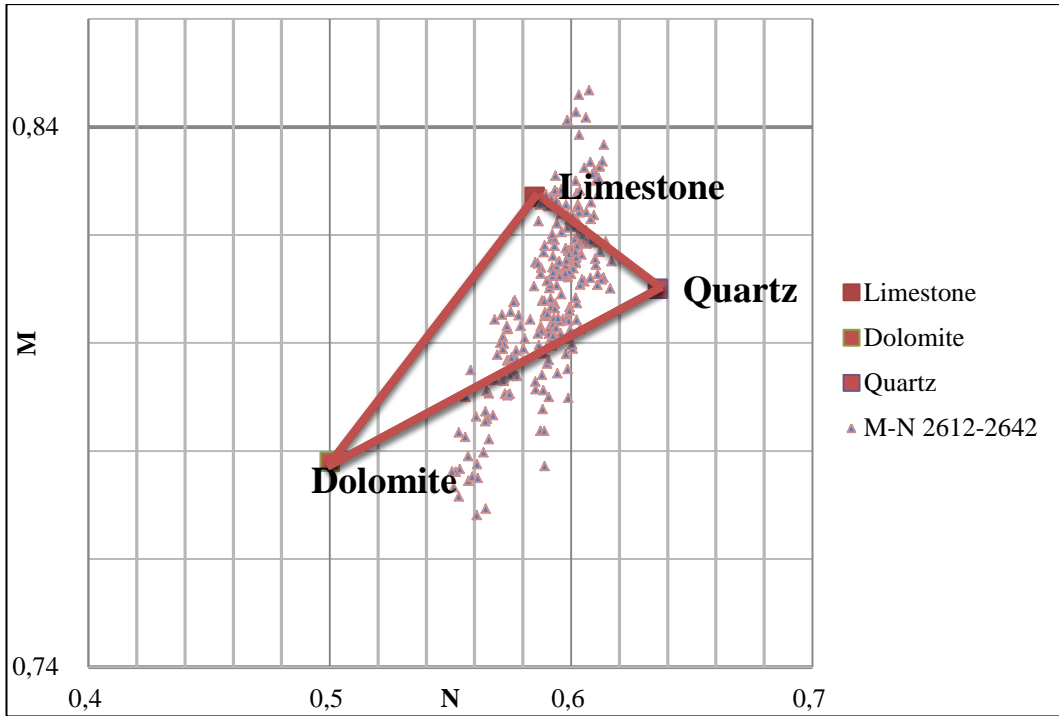


Figure 23 M-N plot for Karaboğaz formation

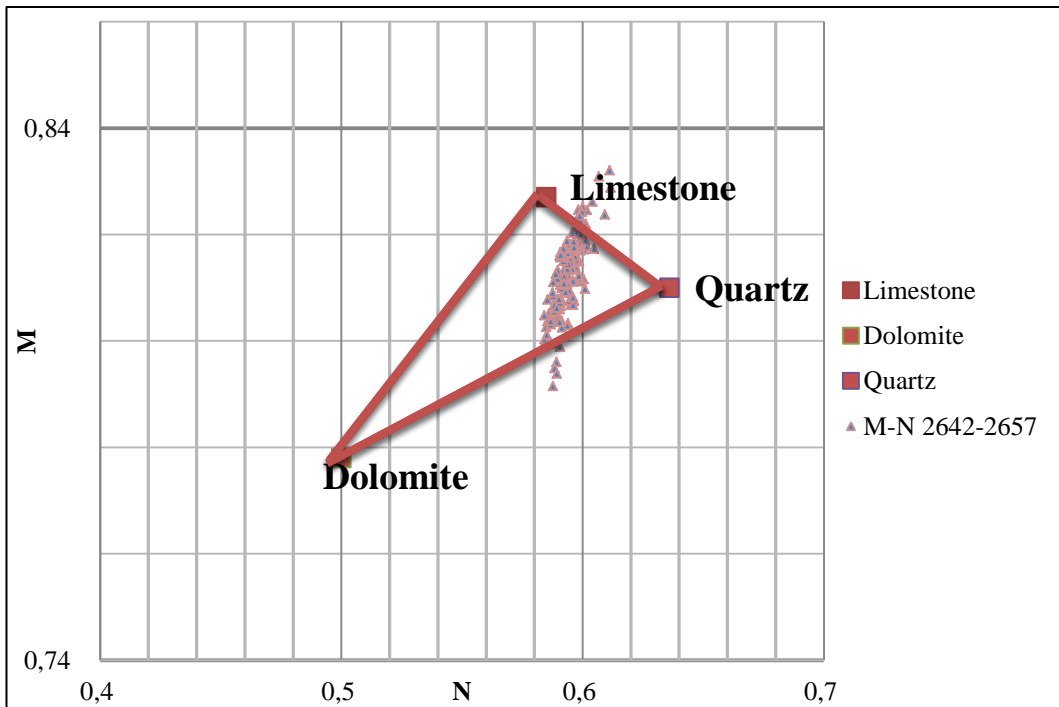


Figure 24 M-N plot for Karababa formation

Table 3 XRD analysis result [31]

| SAMPLE taken from | | | MINERAL COMPOSITION (% VOLUME) (± 4) | | | |
|-------------------|-----------|-----------|---|----------|---------|-----------|
| | | | Quartz | Dolomite | Calcite | Clay+Mica |
| Core No | Depth (m) | Formation | | | | |
| 1 | 2565.30 | Karaboğaz | 96 | | 4 | - |
| 2 | 2566.40 | Karaboğaz | | 6 | 94 | - |
| 3 | 2568.60 | Karaboğaz | | 4 | 96 | - |
| 4 | 2571.15 | Karaboğaz | | 4 | 96 | - |
| 5 | 2583.20 | Karababa | 10 | 5 | 85 | - |

5.3 Elastic Constants of Sayındere, Karaboğaz and Karababa Formations

5.3.1 Elastic Constants by Well Logs

The purpose of this section is to obtain average values of the rock strength parameters for Sayındere, Karaboğaz and Karababa formations. The necessary well logs for this calculation are GR log, DSI log (Figure 25) and Density log. The well logs from X-12 well are analyzed and Poisson's Ratio, Shear Modulus (Figure 27), Young's Modulus, Bulk Modulus, Bulk Compressibility are obtained assuming an infinite, isotropic, homogeneous and elastic medium.

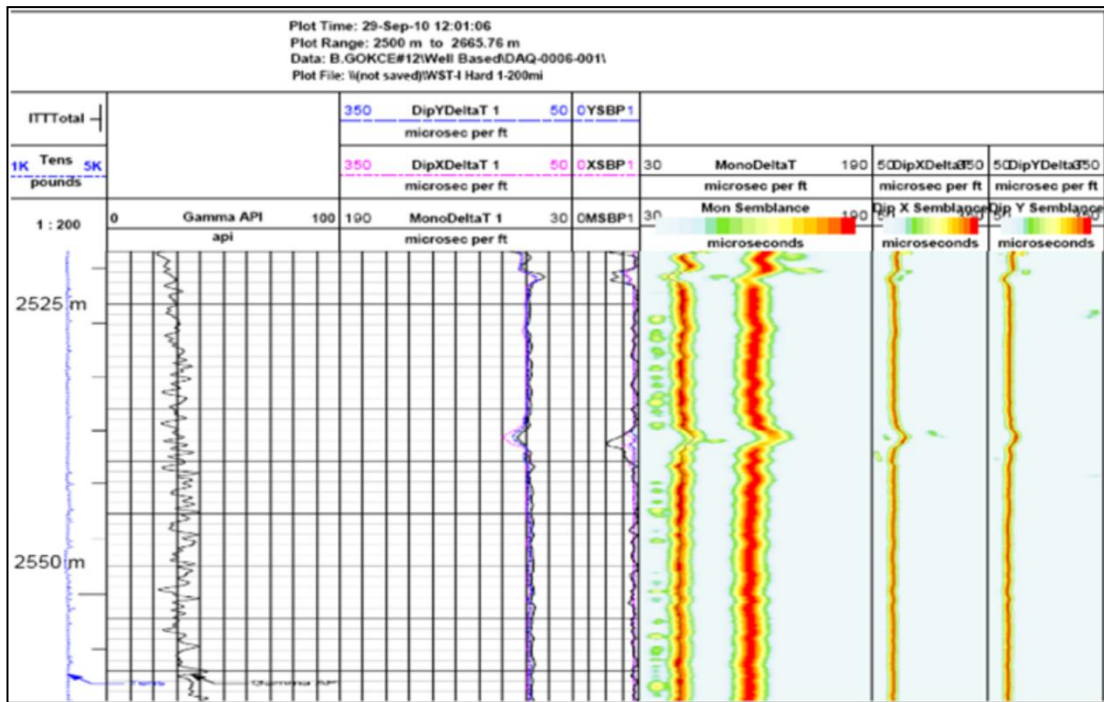


Figure 25 A section from the DSI log [29]

Measured shear and compressional times converted to shear and compressional velocities and graphed (Figure 26). Due to the micro cracks and fractures of Karaboğaz formation there are deviations in measured time values, which can also be seen from Figure 27 Shear Modulus graph. As stated before shear modulus is a measure of sample's resistance against shear deformation. At the points of fractures value of the shear modulus is decreasing.

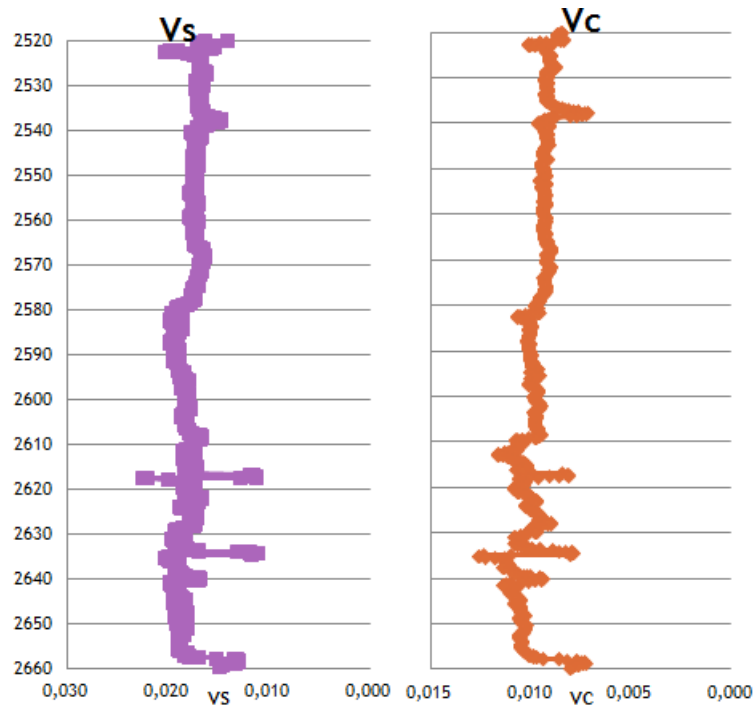


Figure 26 Shear and compressional velocities

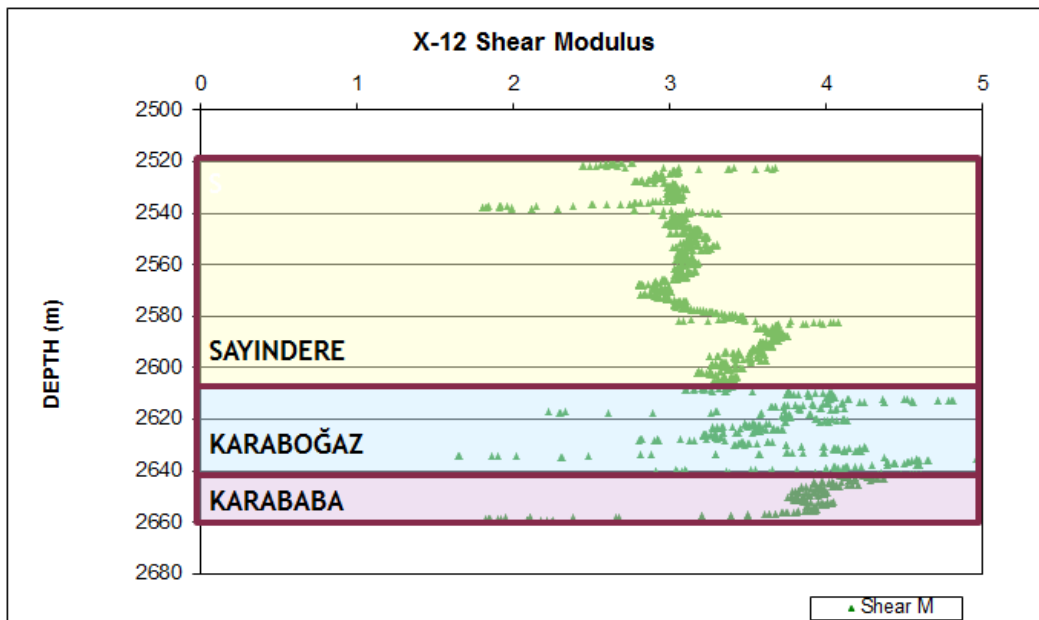


Figure 27 Shear modulus for Sayindere, Karaboğaz and Karababa formations

5.3.2 Sample Calculation of Dynamic Elastic Parameters

| | |
|---------------------------------|------------------|
| Well name | : X-12 |
| Depth | : 2525 m. |
| GR | : 12,7 APIU |
| GR _{clean} | : 2 APIU |
| GR _{shale} | : 90 APIU |
| ρ _b | : 2.68 gr/cc |
| t _c | : 59,65 μsec/ft |
| t _s / t _c | : 1.90 |
| t _s | : 110,84 μsec/ft |

$$\text{Shale Index} = \frac{(GR - GR_{\text{Clean}})}{(GR_{\text{Shale}} - GR_{\text{Clean}})} \quad (5.3)$$

$$\text{Shale Index} = \frac{(12,7-2)}{(90-2)} = 0.12$$

$$\text{(Older Rocks), } V_{\text{sh}} = 0.333 (2^{2*0.12} - 1.0) \quad (5.4)$$

$$\text{Corrected } V_{\text{sh}} = 0.333 (2^{2*0.12} - 1.0) = 0.06$$

$$\text{Poisson's ratio} = \frac{0.5 (t_s/t_c)^2 - 1}{(t_s/t_c)^2 - 1} \quad (5.5)$$

$$v = \frac{0.5 (1.86)^2 - 1}{(1.86)^2 - 1} = 0.3$$

$$\text{Shear Modulus} = \frac{\rho_b}{t_s^2} \times a \quad (5.6)$$

$$G = \frac{2.68}{110,8^2} \times 1.34 \times 10^{10} = 2,92 \times 10^6 \text{ psi}$$

$$\text{Young's modulus} = 2G (1 + v) \quad (5.7)$$

$$E = 2 \times 2,92 \times 10^6 (1 + 0.3) = 7,6 \times 10^6 \text{ psi}$$

$$\text{Bulk modulus} = \rho_b \left[\frac{1}{t_c^2} - \frac{4}{3t_s^2} \right] \times a \quad (5.8)$$

$$K_b = \frac{\left[\frac{1}{59,65^2} - \frac{4}{3(110,84)^2} \right]}{3} \times 1.34 \times 10^{10} = 6,19 \times 10^6 \text{ psi}$$

$$\text{Bulk compressibility} = \frac{1}{K_b} \quad (5.9)$$

$$c_b = \frac{1}{6,19 \times 10^6} = 0.16 \times 10^{-6} \text{ psi}^{-1}$$

Average values of “ t_s/t_c ” and “ ρ_b ” for each formation were determined (Table 4) from DSI log and Density Log and these values were generalized for Sayindere, Karaboğaz and Karababa formations.

Table 4 Generalized bulk density and t_s/t_c values

| Formation | t_s/t_c | ρ_b , gr/cc |
|-----------|-----------|---------------------|
| Sayindere | 1,86 | 2,656 |
| Karaboğaz | 1,74 | 2,631 |
| Karababa | 1,79 | 2,662 |

5.3.2 Elastic Constants by Laboratory Tests

The purpose of this section is to obtain average values of the rock strength parameters for Karaboğaz and Karababa formations to check the consistency with the values calculated by well logs. The cores are taken from X-11 well. For the experiments four core samples taken, three of them from Karaboğaz and one of them from Karababa (Figure 29). The necessary data for this calculation is density values of the samples collected from cores, shear and compressional times measured by sonic viewer. Density values were measured by pycnometer, t_s-t_c values measured

by sonic viewer are presented in Table 4. Unlike t_s the measurement of t_c is related with the saturation. As the saturation increased the measured time will also increase.

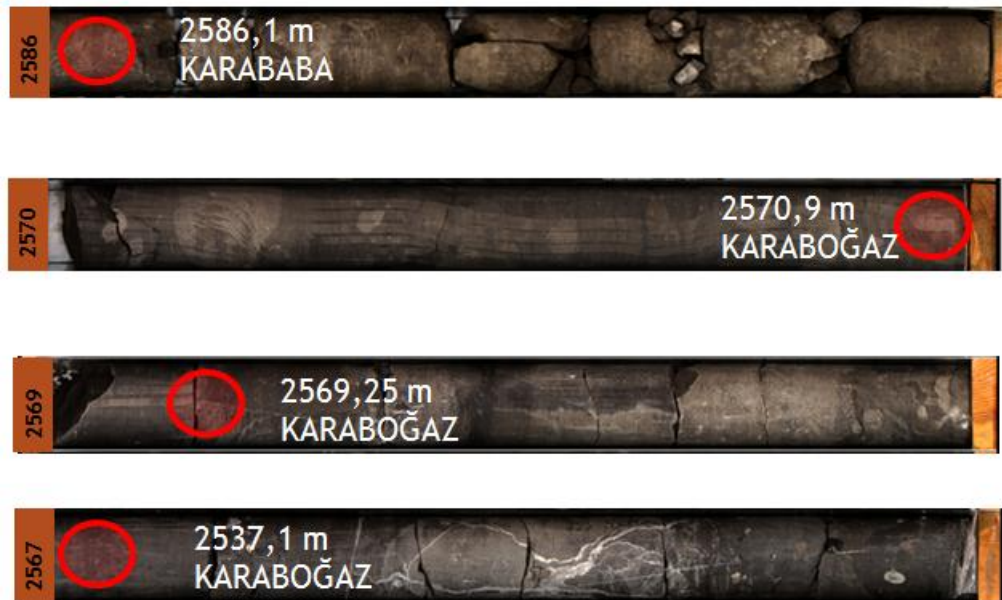


Figure 28 X-11 Well cores and sample places.

Table 5 Measured values of density and t_s/t_c [31]

| FORMATION | DEPTH (m) | DENSITY (gr/cc) | Measured t_c $\mu\text{sec}/\text{ft}$ | Measured t_s $\mu\text{sec}/\text{ft}$ |
|-----------|--------------|--------------------|--|--|
| KARABOĞAZ | 2.567,1 | 2,61 | 53,48 | 105,86 |
| KARABOĞAZ | 2.569,2 | 2,65 | 56,17 | 94,59 |
| KARABOĞAZ | 2.570,9 | 2,77 | 66,52 | 112,71 |
| KARABABA | 2.598,4 | 2,67 | 54,57 | 84,03 |

After the measurement elastic parameters calculated and results are presented in Table 6.

Table 6 Elastic parameters for X-11 well

| FORMATION | DEPTH (m) | POISSON'S RATIO | SHEAR MODULUS psi (*10 ⁶) | YOUNG'S MODULUS psi (*10 ⁶) | BULK MODULUS Psi (*10 ⁶) | BULK COMPR. (*10 ⁻⁶) |
|-----------|--------------|--------------------|--|--|---|--|
| KARABOĞAZ | 2.567,1 | 0,33 | 3,12 | 8,3 | 8,07 | 0,12 |
| KARABOĞAZ | 2.569,2 | 0,23 | 3,96 | 9,7 | 5,96 | 0,17 |
| KARABOĞAZ | 2.570,9 | 0,23 | 2,92 | 7,2 | 4,49 | 0,22 |
| KARABABA | 2.598,4 | 0,14 | 5,06 | 11,5 | 5,25 | 0,19 |

5.4 Calculation of Minimum and Maximum Mud Weights

In this section, minimum mud weights required to prevent borehole collapse and maximum allowable mud weights for Sayındere, Karaboğaz and Karababa formations of X-12 and X-11 well were calculated. To do this, Mohr-Coulomb criterion was used, assuming there is no fluid communication between the wellbore and the formation.

$$\text{Case 'a'} \quad \sigma_{\theta} \geq \sigma_z \geq \sigma_r \quad P_w \leq P_f + \frac{2(\sigma_h - P_f) - C_o}{\tan^2 \beta + 1} \quad (5.10)$$

$$\text{Case 'b'} \quad \sigma_z \geq \sigma_{\theta} \geq \sigma_r \quad P_w \leq P_f + \frac{[\sigma_v - P_f - C_o]}{\tan^2 \beta} \quad (5.11)$$

$$\text{Case 'c' } \sigma_z \geq \sigma_r \geq \sigma_\theta \quad P_w \geq P_f + 2(\sigma_h - P_f) - \frac{[\sigma_v - P_f - C_o]}{\tan^2 \beta} \quad (5.12)$$

$$\text{Case 'd' } \sigma_r \geq \sigma_z \geq \sigma_\theta \quad P_w \geq P_f + \frac{2(\sigma_h - P_f) \tan^2 \beta + C_o}{\tan^2 \beta + 1} \quad (5.13)$$

$$\text{Case 'e' } \sigma_r \geq \sigma_\theta \geq \sigma_z \quad P_w \geq P_f + (\sigma_v - P_f) \tan^2 \beta + C_o \quad (5.14)$$

$$\text{Case 'f' } \sigma_\theta \geq \sigma_r \geq \sigma_z \quad P_w \leq P_f + 2(\sigma_h - P_f) - (\sigma_v - P_f) \tan^2 \beta - C_o \quad (5.15)$$

By using the equations for shear failure and tensile failure, all possible cases were checked for every 0.1 m. section of the formations. Case 'c', 'd' and 'e' were checked to determine the minimum required well pressure for each section. To determine the maximum allowable well pressure for each section, case 'a', 'b' and 'f' were checked. Then the minimum required mud weight and maximum allowable mud weight were calculated for each section by using;

$$MW = \frac{1}{0.052} \times \frac{P_w}{D} \quad (5.16)$$

Where D is depth in ft., well pressure is in psi and mud weight is in ppg. Calculated min and maximum mud weights are graphed (Figure 29) and average values are shown. Since Sayındere, Karaboğaz and Karababa formation are very stable formations (drilled with a mud weight of 66-68 ppcf) calculated minimum mud weights are very low.

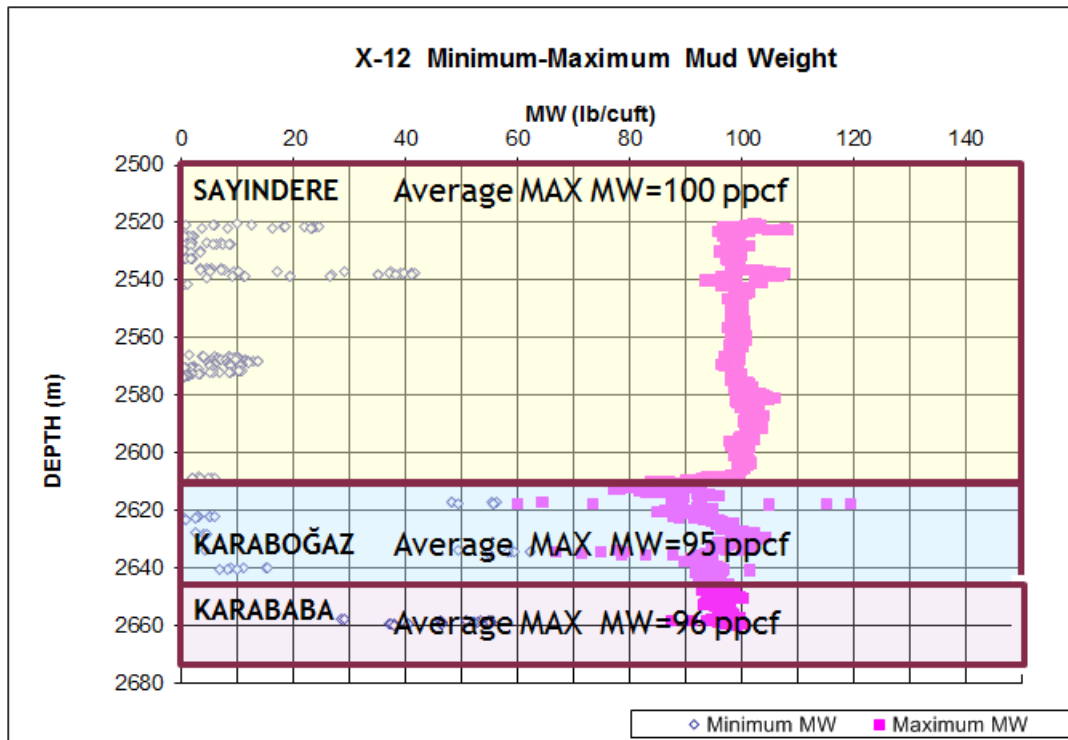


Figure 29 X-12 Min-Max mud weights

For the maximum mud weights of Karaboğaz there are some anomalies at 2616-2617 m and 2634 m. At these depths calculated Poisson's Ratio values are negative. According to the literature negative Poisson's Ratio is indication of anisotropy and exhibit the effect only in some directions [24]. Rocks can be anisotropic; however it is possible that the effects reported in rocks with micro cracks are due to non-affine deformation in the opening of the micro cracks [21].

The calculated maximum mud weight for Sayındere formation is supported by a Formation Integrity Test done in the X-11 well, Sayındere formation. According to the test at 110 ppcf the formation has not formed any fracture. The related data

which belongs to the test can be seen from Figure 30. The value of $R^2=0.9977$ shows that the line still perfectly fits. Since it is known that at the LOP wellbore pressure line begins to be not linear, the conducted test is not LOT. This shows the mud weight that causes the formation leaks off is higher than 110 ppcf.

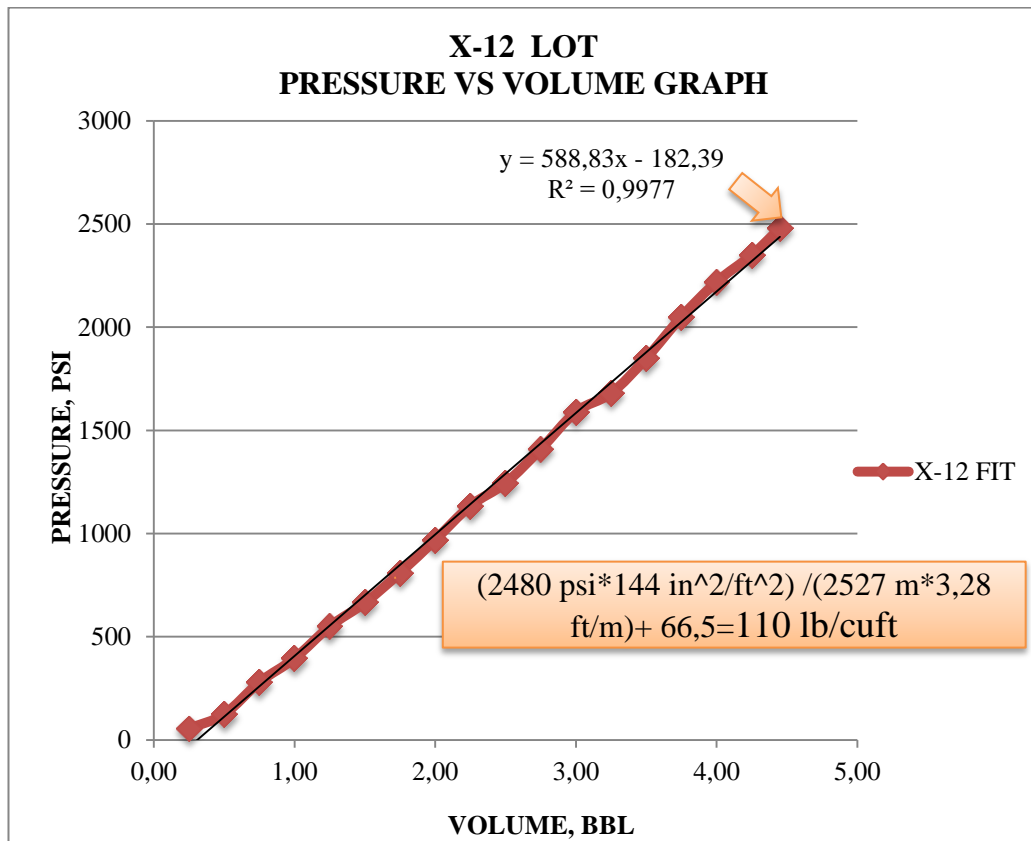


Figure 30 X-12 Formation integrity test graph

For the calculations of mud weights from laboratory data there is one more needed measurement which is uniaxial compressive strength. The measured values of uniaxial compressive strength and cohesion angles are tabulated (Table 7). The discrepancies of the measured values are related with sample porosities. Measured porosity values are 3.7%, - , 3,7% and 4.9% [31]. According to the measured porosity values since second sample has no porosity it needs higher compressive strength relative to others.

Table 7 Uniaxial compressive strength and cohesion angles [31]

| FORMATION | DEPTH (m) | UNIAXIAL COMP.STR. (psi) | COHESION ANGLES (degree) |
|-----------|--------------|--------------------------------|--------------------------------|
| KARABOĞAZ | 2.567,10 | 18,6 | 75 |
| KARABOĞAZ | 2.569,20 | 32,6 | 65 |
| KARABOĞAZ | 2.570,90 | 17,7 | 88 |
| KARABABA | 2.598,40 | 22 | 75 |

Calculated maximum mud weight values from laboratory tests are tabulated (Table 8) and they are in consistency with the values calculated from well logs.

Table 8 Maximum mud weights from laboratory tets

| FORMATION | DEPTH, m | MAXIMUM MW from LAB. DATA, lb/cuft | AVERAGE OF MAXIMUM MW from WELL LOG DATA, lb/cuft |
|-----------|----------|--|--|
| KARABOĞAZ | 2567,1 | 104,6 | 95 |
| KARABOĞAZ | 2569,2 | 86,6 | |
| KARABOĞAZ | 2570,9 | 90,2 | |
| KARABABA | 2586,1 | 89,8 | 96 |

5.4.1 Sample calculation

Well name : X-12
 Depth : 2525 m = 8284 ft
 GR : 12,7 APIU
 GR_{clean} : 2 APIU
 GR_{shale} : 90 APIU
 ρ_b : 2.68 gr/cc
 t_c : 59,65 μsec/ft
 t_s / t_c : 1.90
 t_s : 110,84 μsec/ft

$$\text{Formation pore pressure} = 0.465 \text{ psi/ft} \times \text{Depth} \quad (5.17)$$

$$P_f = 0.465 \times 2525 \times 3.28 = 3851 \text{ psi}$$

$$P_{ob} = \int_0^D \rho(D) g dD \quad (5.18)$$

Overburden pressure = 2520.3 m x 3,28 ft/m + 17,62 = 8284 psi (by using density log data)

$$\sigma_h = \frac{\nu}{(1 - \nu)} (P_{ob} - P_f) + P_f \quad (5.19)$$

$$\text{Horizontal stress} = \frac{0.3}{(1 - 0.3)} (8284 - 3851) + 3851 = 5716 \text{ psi}$$

$$C_o = \frac{2 \cos \Phi}{1 - \sin \Phi} \times \frac{0.026 E}{c_b \times 10^6} [0.008 V_{\text{clay}} + 0.0045 (1 - V_{\text{clay}})] \quad (5.20)$$

$$C_o = \frac{2 \cos (30^\circ)}{1 - \sin (30^\circ)} \times \frac{0.026 \times 7,6 \times 10^6}{0.16 \times 10^{-6} \times 10^6} [0.008 \times 0.06 + 0.0045 (1 - 0.06)]$$

$$C_o = 19112 \text{ psi}$$

5.4.1.1 Calculation of Minimum Required Mud Weight

For the calculation of minimum mud weight assumptions are wellbore is vertical, stresses acting horizontally are isotropic and wellbore is not permeable. In addition; mud cake on the wellbore is perfect and well pressure can not affect the pore pressure.

$$\sigma_r = P_w \quad (5.21)$$

$$\sigma_\theta = 2\sigma_h - P_w \quad (5.22)$$

$$\sigma_z = \sigma_v \quad (5.23)$$

$$\text{Case 'a'} \quad \sigma_\theta \geq \sigma_z \geq \sigma_r \quad P_w \leq P_f + \frac{2 (\sigma_h - P_f) - C_o}{\tan^2 \beta + 1} \quad (5.24)$$

$$\text{Case 'b' } \sigma_z \geq \sigma_\theta \geq \sigma \quad P_w \leq P_f + \frac{[\sigma_v - P_f - C_o]}{\tan^2 \beta} \quad (5.25)$$

$$\text{Case 'c' } \sigma_z \geq \sigma_r \geq \sigma_\theta \quad P_w \geq P_f + 2(\sigma_h - P_f) - \frac{[\sigma_v - P_f - C_o]}{\tan^2 \beta} \quad (5.26)$$

$$\text{Case 'd' } \sigma_r \geq \sigma_z \geq \sigma_\theta \quad P_w \geq P_f + \frac{2(\sigma_h - P_f) \tan^2 \beta + C_o}{\tan^2 \beta + 1} \quad (5.27)$$

$$\text{Case 'e' } \sigma_r \geq \sigma_\theta \geq \sigma_z \quad P_w \geq P_f + (\sigma_v - P_f) \tan^2 \beta + C_o \quad (5.28)$$

$$\text{Case 'f' } \sigma_\theta \geq \sigma_r \geq \sigma_z \quad P_w \leq P_f + 2(\sigma_h - P_f) - (\sigma_v - P_f) \tan^2 \beta - C_o \quad (5.29)$$

Case 'a' in Table assumes $\sigma_\theta \geq \sigma_z \geq \sigma_r$ and to prevent shear failure,

$$P_w \leq P_f + \frac{2(\sigma_h - P_f) - C_o}{\tan^2 \beta + 1} \quad (5.30)$$

$$P_w \leq 3851 + \frac{2(5716 - 3851) - 19112}{\tan^2 60 + 1}$$

Minimum well pressure = 6 psi

$$\sigma_{\theta} = 2\sigma_h - P_w \quad (5.31)$$

$$\sigma_{\theta} = 2 \times 5716 - 6$$

$$\sigma_{\theta} = 11427 \text{ psi}$$

$$\sigma_{\theta} = 11407 \geq \sigma_z = 8284 \text{ psi (the assumption of case 'a' is valid)}$$

$\sigma_{\theta} \geq \sigma_z \geq \sigma_r$ is valid when 6 psi is the minimum required well pressure at 2525 m to prevent shear failure.

Case 'b' assumes $\sigma_z \geq \sigma_{\theta} \geq \sigma_r$ and to prevent shear failure,

$$P_w \leq P_f + \frac{[\sigma_v - P_f - C_o]}{\tan^2 \beta} \quad (5.32)$$

$$P_w \leq 3851 + \frac{[8284 - 3851 - 19112]}{\tan^2 60}$$

$$P_w \leq -1042 \text{ psi}$$

$$\sigma_{\theta} = 2\sigma_h - P_w \quad (5.33)$$

$$\sigma_{\theta} = 2 \times 5716 + 1042$$

$$\sigma_{\theta} = 12474 > \sigma_z = 8284 \text{ psi (the assumption of case 'b' is failed)}$$

Since $\sigma_z \geq \sigma_{\theta} \geq \sigma_r$ is not valid, then -1042 psi is not the minimum required well pressure at 2525 m.

$$MW_{\min} = \frac{1}{0.052} \times \frac{P_w}{D} \quad (5.34)$$

$$\text{Minimum required mud weight} = \frac{1}{0.052} \times \frac{6}{2525 \times 3.28} = 0.14 \text{ ppg} = 1.0472 \text{ ppcf}$$

5.4.1.2 Calculation of Maximum Allowable Mud Weight

Case 'c' assumes $\sigma_z \geq \sigma_r \geq \sigma_\theta$ and to prevent shear failure,

$$P_w \geq P_f + 2(\sigma_h - P_f) - \frac{[\sigma_v - P_f - C_o]}{\tan^2 \beta} \quad (5.35)$$

$$P_w \geq 3851 + 2 \times (5716 - 3851) - \frac{[8284 - 3851 - 19112]}{\tan^2(60^\circ)}$$

$$P_w \geq 12474 \text{ psi}$$

$$\sigma_\theta = 2\sigma_h - P_w \quad (5.36)$$

$$\sigma_\theta = 2 \times 5716 - 12474$$

$\sigma_\theta = -1042 \text{ psi} < \sigma_r = 12474 \text{ psi}$ however $\sigma_r = 12474 \text{ psi} > \sigma_z = 8284 \text{ psi}$ not certifies $\sigma_z \geq \sigma_r \geq \sigma_\theta$.

So, assumption of case 'c' is failed.

Case 'd' assumes $\sigma_r \geq \sigma_z \geq \sigma_\theta$ and to prevent shear failure,

$$P_w \geq P_f + \frac{2(\sigma_h - P_f) \tan^2 \beta + C_o}{\tan^2 \beta + 1} \quad (5.37)$$

$$P_w \geq 3851 + \frac{2(5716 - 3851) \tan^2 60 + 19112}{\tan^2 60 + 1}$$

$$P_w \geq 11427 \text{ psi}$$

$$\sigma_\theta = 2\sigma_h - P_w \quad (5.38)$$

$$\sigma_\theta = 2 \times 5716 - 11427$$

$$\sigma_\theta = 6 \text{ psi}$$

$$\sigma_\theta = 6 \geq \sigma_z = 8284 \text{ psi (the assumption of case 'd' is valid)}$$

$\sigma_r \geq \sigma_z \geq \sigma_\theta$ $11427 \geq 8284 \geq 6$ is valid when 11427 psi is the minimum required well pressure at 2525 m to prevent shear failure.

To determine the maximum allowable mud weight, tensile failure criterion should also be checked.

$$P_w = 2\sigma_h - P_f + T_o \quad (5.39)$$

$$P_w = 2 \times 5716 - 3851 + 0$$

$$P_w = 7582 \text{ psi}$$

Then, maximum allowable well pressure is 7582 psi and,

$$MW = \frac{1}{0.052} \times \frac{P_w}{D} \quad (5.40)$$

$$MW = \frac{1}{0.052} \times \frac{7582}{2525 \times 3.28}$$

Maximum Allowable Mud Weight = 17.6 ppg = 127.17 ppcf

CHAPTER 6

CONCLUSIONS

The purpose of this study was to show the use of geomechanical wellbore stability theory by using well logs, laboratory data and linear elastic theory in constructing mud weight window to prevent stability problems in Sayındere, Karaboğaz and Karababa formations.

To begin with, lithology was identified by the analysis of drill cuttings, well log data and X-Ray diffractometer. The composition of each formation is identified, namely, Sayındere is composed of limestone and Karaboğaz formation is composed of limestone and chert and Karababa formation is composed of mostly limestone and with a few chert. To support the results obtained from X-12 well drill cuttings, well logs are used. Moreover, X-11 well core samples are analysed by XRD. All the analysis results supports each other. In the second part of the study, X-12 well elastic rock parameters are calculated by using GR, DSI and Density log data and the values are supported by experimental measurements of density, and t_s-t_c values from X-11 well core samples. The density, shear and compressional time values are generalized for X field Sayındere, Karaboğaz and Karababa formations. Generalized density values for Sayındere, Karaboğaz, Karababa formations are 2.656, 2.631, 2.662 gr/cc and generalized values for t_s/t_c are 1.86, 1.74, 1.79 respectively. In the final part of the study, minimum and maximum mud weights for the studied formations are determined by using Mohr-Coulomb criterion and assuming no communication between the borehole and the formation. The calculated values from X-12 well logs and X-11 well core samples' experimental data for mud weights are in consistency. Moreover, the calculated value for Sayındere formation is supported by a formation integrity test. Since the studied formations does not have any stability problem, the

calculated minimum mud weight values certifies the practical values. The average values of maximum mud weights for Sayındere, Karaboğaz and Karababa formations are 100 ppcf, 95 ppcf and 96 ppcf respectively.

In conclusion, to reduce drilling costs and hazardous conditions the described methodology allows prediction, prevention and reduction of wellbore instability conditions. Furthermore, for the studied field by using generalized values of shear time and compressional time the dynamic elastic parameters can be calculated for the rest of wells without recording any new DSI log.

REFERENCES

- [1] Al Ajmi, Zimmerman, R.W.: "Stability Analysis of Deviated Boreholes Using the Mogi-Coulomb Failure Criterion, With Applications to Some Oil and Gas Reservoirs" paper SPE 104035, Imperial College, London

- [2] Addis MA: "The Stress-Depletion Response of Reservoirs," paper SPE 38720, presented at the SPE Annual Technical Conference and Exhibition, San Antonio, Texas, October 5-8,1997.

- [3] Geertsma J: "Land Subsidence Above Compacting Oil and Gas Reservoirs," paper SPE 3730, presented at SPE-AIME European Spring Meeting, Amsterdam, Nlay 16-18, 1972.

- [4] BR and Yale DP: "Constitutive Modeling of Deformation and Permeability: Relationships between Critical State and Micromechanics," paper SPE/ISRM 78189, presented at the SPE/ISRM Rock Mechanics Conference, Irving, Texas, October 20-23, 2002.

- [5] Doornhof D, Iristiansen TO, Nagel NB, Pattillo PD and Sayers C: "Compaction and Subsidence," Oilfield Review IS, no. 3 (Autumn 2006): 50-68.

- [6] Bell, J.S.: "Practical methods for estimating in situ stresses for borehole stability applications in sedimentary basins", J Pet Sci Eng (2003) 38[3-4]:111-119.

- [7] Fairhurst, C.: "Stress estimation in rock: a brief history and review", Int J Rock Mech Min Sci (2003) 40[7-8]:957-973.

- [8] Fjaer, E. et al.: "Petroleum Related Rock Mechanics", Elsevier, Amsterdam, 1992, 338.

- [9] Amadei, B. and Stephenson, O.: "Rock Stress and its Measurement", Chapman & Hall, London, 1997.
- [10] Gough, D.I. and Bell, J.S.: "Stress Orientations from Borehole Wall Fractures with Examples from Colorado, East Texas, and Northern Canada", *Can J Earth Sci* (1982) 19[7]:1358-1370. 29. Zoback, M.D.: "Wellbore breakouts and in situ stress", *Geophyte Res-Sol Earth Plan*, (1985) 90[NB7]:5523-5530.
- [11] Choi SK and Tan CP: "Modeling of Effects of Drilling Fluid Temperature on Wellbore Stability," *Proceedings, SPE/ISRM Rock Mechanics in Petroleum Engineering Symposium, Trondheim, Norway (July 8-10, 1998): 471-477.*
- [12] Gazaniol D, Forsans T, Boisson MJF and Piau JM:" Wellbore Failure Mechanisms in Shales: Prediction and Prevention," paper SPE 28851, presented at the SPE European Petroleum Conference, London, October 25-27, 1994.
- [13] Savers CM, Kisra S, Tagbor K, Dahi Taleghani A and Ariachi J: "Calibrating the Mechanical Properties and In-Situ Stresses Using Acoustic Radial Profiles," paper SPE 110089-PP, presented at the SPE Annual Technical Conference and Exhibition, Anaheim, California, USA, November 11-14, 2007.
- [14] Addis T, Last N, Boulter D, Roca-Ramisa L and Plumb D: "The Quest for Borehole Stability in the Cusiana Field, Colombia," *Oilfield Reviews*, no. 2 & 3 (April/July 1993): 33-43.
- [15] Aoki T, Tan CP and Bamford WE: "Stability Analysis of Inclined Wellbores in Saturated Anisotropic Shales," in Siriwardane HJ and Zaman M.: *Computer Methods and Advances in Geomechanics: Proceedings of the Eighth International Conference on Computer Methods and Advances in Geomechanics, Morgantown, West Virginia, USA, May 22-28, 1994. Rotterdam, the Netherlands: A.A. Balkema (1994):2025-2030.*

- [16] Yamamoto K, Shioya Y, Matsunaga TY, Kikuchi S and Tantawi L "A Mechanical Model of Shale Instability Problems Offshore Abu Dhabi," paper SPE 78494, presented at the 10th Abu Dhabi International Petroleum Exhibition and Conference, Abu Dhabi, UAE, October 13-16, 2002

- [17] Tittman, J.: "Radiation Logging: Physical Principals", presented at University of Kansas Petroleum Engineering Conference, April 2-3, 1956.

- [18] Serra, O.: "Fundamentals of Well Log Interpretation", Elsevier Science Publishing Co., Amsterdam, 1984.

- [19] Schlumberger : "Log Interpretation, Volume 1, Principles", Schlumberger Limited, New York, 1972

- [20] Doveton, J.: "Basics Of Oil & Gas Log Analysis", Kansas Geological Survey, Doveton, 1999.

- [21] Winkler KW, Liu HL and Johnson DJ: "Permeability and Borehole Stoneley Waves: Comparison Between Experiment and Theory", Geophysics54

- [22] Haldorsen J, Johnson D: "Borehole Acoustic Waves", Oilfield Review, Ridgefield, Connecticut, 2006, 34

- [23] Jaeger, J.C. and Cook, N.G.W.: "Fundamentals of Rock Mechanics", Chapman and Hall Edition, London, 1979.

- [24] Brown, S., Swan, G., Jeffrey, R.: "Basics of Failure Mechanics", The Technical Review, Volume 34, Number 3, Schlumberger Limited, U.S.A., October 1986.

- [25] Dewan, J.T.: “Essentials of Modern Open-Hole Log Interpretation”, Pennwell Publishing Company, Tulsa, Oklahoma, 1983.
- [26] Metu Central Laboratory, <http://www.centrallab.metu.edu.tr/?q=en/node/152>, last visited on May 2011.
- [27] Comenius University in Bratislava, http://www.fpharm.uniba.sk/fileadmin/user_upload/english/Fyzika/Density_determination_by_pycnometer.pdf, last visited on April 2011.
- [28] Earth Products China Limited, <http://www.epccn.com/en/productinfo605.html>, last visited on April 2011.
- [29] TPAO Production Department
- [30] Yılmaz, E.: “Güneydoğu Anadolu Bölgesi Otokon ve Allokon Birimler Stratigrafi Adlama Sözlüğü”, Türkiye Petrolleri Anonim Ortaklığı Araştırma Merkezi Grubu Başkanlığı Eğitim Yayınları No:31, Ankara, Şubat 1997
- [31] TPAO Research Center